Evaluation of Reinforced Concrete Tall Buildings with End Shear Walls Subjected to Sequences Far from the Fault

Mehran Akhavan Salmassi [a], Ali kheyroddin [b*], Ali Hemmati[c]

[a] *Ph.D. Candidate of Structural engineering, Seismic Geotechnical and High Performance Concrete Research Center, Department of Civil Engineering, Semnan Branch, Islamic Azad university, Semnan, Iran.*
(E-mail: M.Akhavan.s@stu.semnaniau.ac.ir)(Mobile: +98-9155947822) (Telephone: + 98 -5137640538)

[b] *Professor of structural engineering, Member of Center of Excellence for Engineering and Management of Civil Infrastructures, University of Tehran, Iran, Faculty of Civil Engineering, Semnan University, Iran.*
(E-mail: kheyroddin@semnan.ac.ir)(Mobile:+98-9121318121)(Telephone: + 98 -2331535220)

[c] *Assistant Professor of structural engineering, Seismic Geotechnical and High Performance Concrete Research Center, Department of Civil Engineering, Semnan Branch, Islamic Azad university, Semnan, Iran.*
(E-mail: ali.hemmati@semnaniau.ac.ir) (Mobile:+98-9122311936) (Telephone: + 98 – 2333654041)

Abstract.

Many parameters affect the behavior of tall buildings under seismic loads, some of which are the main shock-after shock records and using some lateral load resistance systems in reinforced concrete tall buildings. End shear walls are a kind of shear walls, connecting their end in tall buildings. This study was conducted on two 30-story reinforced concrete structures, which were subjected to sequences of far fault records and analyzed by the nonlinear time history analysis. The results indicated a 51% decrease in maximum inter-story drift in 30 stories with end shear walls under sequence records. The normal Q-Q plots (quantile-quantile plot) presented approximately 20% reduction in the excepted normal domain in X and Y directions, respectively, in 30 stories with end shear walls. The kurtosis coefficient declined by 61 and 92% in the X and Y directions in 30-story structure end shear walls, respectively. Therefore, the end shear wall increased the confinement effects by decreasing the dispersion data of inter-story drift and improving seismic behavior.

Corresponding author: Ali Kheyroddin *(E-mail: kheyroddin@semnan.ac.ir)(Mobile:+989121318121)(Telephone: + 98 -2331535220)*

Keywords:

Tall Buildings; End Shear Wall; Nonlinear Time History Analysis; Sequence records; Far Fault.

1. Introduction

Studies have suggested various lateral load systems methods, revealing the significant role of seismic behavior on high-rises. RC shear walls contribute to the proper performance of structures. As a result of severe tensions at the end flanges of the shear walls, the parameter was improved by connecting the end walls in all stories. The system has become more stable and complex by adding the end shear wall. Furthermore, the layout of the core walls gave the overall structure system torsion strength and hardness, and the extension of the corners limited floor deflection.

Shen et al. (2019) conducted a 20-story frame-core tube subject to evaluate the behavior of shear walls in RC structures under sequence records and sequential ground motions and showed the effects of sequential records on the structural design [1]. Jamnani et al. (2018) focused on energy distribution in RC structures subjected to repeated records and found that the effect of sequence earthquakes should be considered in assessing the reliability of structures [2]. In addition, the exceeding probability of a severe damage state rises from 35.3% to 62.1% due to the solid aftershocks by vulnerability assessment of the 32-story structure [3]. Some tall buildings were evaluated by single and multiple peaks, indicating that multiple earthquakes significantly increased the risk of structural frailer [4]. Akhavan Salmassi et al. (2022) assessed the seismic behavior of tall RC buildings with end shear walls. The results showed that the structures with end shear walls had a 50% lower drift ratio than structures without end shear walls [5].

The main shock-aftershock records were also used in studies concerning risk-based assessment. Shokrabadi and Burton (2018) presented the importance of seismic risk from aftershocks in designing structures [6]. In addition, the vulnerability assessment of the structure subjected to the main shock-aftershock showed that the maximum effects of aftershocks can exceed 15% [7]. As a result of the probabilistic model for the RC frame subjected to sequence records, the MS-AS sequence is more uncertain than the MS sequence [8]. Wang et al. (2022) analyzed the fragility of mega-sub controlled structures subjected to sequence records and demonstrated that the additional LRB improved seismic behavior [9] [8]. Zhang et al. (2019) examined the seismic risk of tall buildings by main shock and aftershock. The maximum exceedance probability was related to the coupling beam rotation demand [10]. Zhang and Burton (2021)

studied tall buildings and aftershocks and indicated a framework for optimal decision-making for earthquake damage [11].

On the other hand, Huang et al. (2022) evaluated the seismic performance of RC frames with viscoelastic dampers subjected to sequence records. The IDA results presented a better performance in lead viscoelastic damper, as much as 21.08% in the median after shock PGA demands [12]. Some other studies have investigated tall buildings by nonlinear time history analysis and found recognition patterns to assess the residual structural capacity of damage [13]. In addition, the energy-based method was applied for tall buildings under sequence records. Studies have concluded that the Max ISDR of the shear walls is less than 1% for the main shock and MS-AS records [14].

Moreover, Mantawy and Anderson (2014) investigated tall buildings under sequence records and indicated significant damage due to low-cycle fatigue [15]. Examining the seismic fragility through the IDA method increased the seismic vulnerability under sequence records [16]. While performance-based criteria are desirable for new construction and retrofitting, developing such guidelines can be complicated [17]. Studying the performance of reinforced concrete subjected to sequence records indicated that residual drift and displacement accumulate each aftershock [18]. Tauheed and Alam (2021) suggested that the strength and stiffness decreased with increasing aftershocks [19].

Additionally, the response of reinforced concrete frames with stiffness irregularities under sequence records is analyzed in-depth [20]. Naserpour and Fathi (2022) examined post-tensioned wall frames and indicated that the conventional model posed extensive damage to the structural elements, leading to a damage index of 0.78% and residual drifts of 0.42% under seismic loads [21]. Abdelnaby and Elnashai (2015) assessed numerical modeling and reinforced frames under sequence records and indicated that the sequence earthquake significantly affects earthquake safety [22]. According to the proposed method, synthesized MS-AS sequences produced statistically similar results to as-recorded sequences for buildings subjected to sequence records [23]. In addition, researchers examined the impact of aftershocks on reinforced concrete structures. The findings presented important uncertainty sources for the post-quake decisions through a sensitivity study [24]. Several sequence records have been investigated for their impact

on moment resistance in reinforced concrete frames [25]. In addition, the effects of seismic sequences on structures with dissipative behavior indicated that the result of seismic sequence consideration was essential for design [26]. Reinforced concrete structures subjected to repeated records were also studied and showed that the ductility demands related to sequence records were estimated by combining the corresponding demands of the single records [27].

Based on results from a fragility study and collapse margin capacity evaluation performed on the mega-sub controlled structure system when subjected to a main shock-aftershock excitation, it was determined that the LRB increased the system's seismic resistance [28].

According to the study, "Seismic behavior of reinforced concrete moment resistant structures with concrete shear wall under main shock-aftershock seismic sequences," [29] the medium height model under the seismic sequences showed a considerable increase in the relative displacement (about 25% in some cases), inter-story drift ratio, plastic strain, and residual displacement (42.22 percent rise on average) compared to the structure that was only subjected to the main shock.

Maximum residual relative floor displacements were reduced by around 40% in frames with post-tensioned connections compared to frames with simple moment connections, as determined by an evaluation of flexible steel frame structures with post-tensioned cables to sequences far from fault [30]. Experimental results from shaking table tests on a reinforced concrete frame exposed to main shock-aftershock sequences showed that AIR values increased dramatically with increasing damage to the specimen [31]. Taking into account main shock-aftershock sequences in a seismic fragility assessment of a transmission tower revealed that aftershocks might exacerbate the accumulated damage to the building and decrease its seismic capacity [32]. Fragility analysis of containment structures during main shock-aftershock sequences [33] confirms the need to consider the influence of main shock-damaged levels. A strong aftershock can pollute the efficiency of period normalization, and the impact of a strong aftershock in the near-fault zone on cumulative damage can exceed 20% and reach 40%, as stated in Cumulative Damage of Structures under the Main shock-aftershock Sequences in the Near-fault Region [34]. Research comparing the pounding impacts of different reinforced concrete frames (MRFs) exposed to far-field earthquakes found that shorter MRFs sustained

much more damage than taller structures owing to pounding [35]. An analysis of the effects of modeling uncertainties on the residual drift of steel structures during main shock-aftershock sequences revealed that seismic demands are more sensitive to strength modeling parameters and beam ductility modeling parameters, with these sensitivities increasing by an average of 20% during aftershocks. Aftershocks increase the dispersion of peak drift needs significantly [36]. As documented, aftershocks can increase residual drift demands by as much as 19% for 3-story frames and 15% for 9-story frames at the risk-targeted maximum assessed earthquake MCER level. The procedure can quantitatively estimate the failure probability of a main shock damaged structure during aftershocks considering the influence of the spatial location of the aftershock and the time interval between the main shock and aftershock [37]. This evaluation is based on a spatiotemporal simulation of the regional earthquake sequence.

This literature review aimed to investigate the effect of end shear walls on the nonlinear behavior of RC tall buildings under sequence records. In tall buildings, end shear walls connect the ends of shear walls in all stories, and some parameters, such as confinement and resistance reduction effects, influence the behavior of the buildings. Therefore, this paper evaluates the impact of end shear walls by focusing on mentioned parameters in RC tall buildings subjected to sequence records by nonlinear time history analysis.

2. Material and Methods

2.1 Specifications of structures and materials

Some 30-story buildings were modeled by ETABS software with and without an end shear wall to study how it behaves. A three-dimensional analysis was conducted to determine seismic behavior. The mentioned structures included the reinforced concrete moment frame and shear wall, and the dead and live loads were as much as 170 and 200 kg/m^2, respectively. The floor was a reinforced concrete slab, and the connections of columns and shear walls were rigid at the base. The frame span, floor height, υ , f_c, and f_y are considered as much as 7 m, 4 m, 0.15, 50 MPa, and 400 N/mm^2, respectively. The frames were classified into three dimensions, and OpenSees modeled the structures for nonlinear analysis due to determining frame sections

in ETABS software. Shear walls are shown in red in Figure 1a, while end shear walls are shown in blue in Figs. 1b and c, showing a typical frame elevation.

Tables 1 and 2 represent the buildings and section specifications, respectively.

As mentioned in the figures and specifications, these structures were subjected to seismic analysis after modeling.

2.3 Simulation of the structures

The 30-Story structures were analyzed using linear static analysis, simulated by OpenSees, and their section properties were determined using ETABS software. Due to nonlinear time history analysis, three records were required to apply the structures.

On the other hand, the multi-layer shell element model was used for shear walls. The "ShellMITC4" command was related to the multi-layer shell element model and subdivided the shear wall into a sufficient number of layers. According to the dimensions and distribution of reinforcing bars, Figures 2 and 3 indicated different material properties and multi-layer shell elements. Physically, the stresses at the mid-surface of an orthotropic layer are equal to those over a layer thickness[38].

The specifications of the primary records are indicated in Table 3, which are far-field and site class D. On the other hand, the acceleration time and its response are shown in Figs. 4. Moreover, the graph of energy flux-time of records presents various levels in Figure 5.

Table 4 shows the details of sequence records, including combined details and time duration. In addition, the acceleration-time graphs of sequence records are presented in Fig 6.

Nonlinear time analysis of structures is required in the following.

2.3.1 verification

Para et al. (2019) validated a four-story RC flexural frame using OpenSees algorithms. Figure 7a indicates the detail of the Parra et al. (2019) frame [39]. In Figure 7b and Table 4, Parra et al.'s (2019) maximum base

shear/W (%) and simulation ratios are 10.5% and 11.1%, respectively.

In conclusion, OpenSees performed as intended, with a verification deviation of 5%.

3. Results and discussion

The 30-story structures were modeled with and without end shear walls. The mentioned structures were subjected to three sequence records for nonlinear time history analysis. The drift ratio is one of the significant parameters in seismic behavior in tall buildings. For this purpose, the drift ratios are based on the story presented in Figure 8.

The inter-story drift ratios of sequence records shown in Figure 8a are based on the story of CMF1. As shown in Figure 8a, the gray, blue, and orange colors belong to Combinedsery1, Combinedsery2, and Combinedsery3 records, respectively. The minimum inter-story ratio in Combinedsery1 (7.44E-04), Combinedsery2 (3.8E-04), and Combinedsery3 (1.41E-04) record at the first level. Despite the fluctuation from one to 13-story, the maximum drift ratios were 3.43E-03, 2.34E-03, and 1.26E-03 in Combinedsery1, Combinedsery2, and Combinedsery3 at seven, four, and 25 stories, respectively.

On the other hand, the inter-story drift ratios of records based on the CMF2 story are represented in Figure 8b. The gray, blue, and orange colors were related to Combinedsery1, Combinedsery2, and Combinedsery3 records. The minimum inter-story ratio in Combinedsery1, Combinedsery2, and Combinedsery3 records at the first level were 2.85E-04, 2.92E-04, and 9.95E-05, respectively. In Combinedsery2 and Combinedsery3 records, the maximum inter-story drift ratios were obtained at 1.28E-03 and 7.76E-04 in 9 and 25 levels, respectively. In the Combinedsery1 record, some initial fluctuations led to 24 levels of 1.67E-03.

Accordingly, the inter-story drift ratio is based on CMF1 and CMF2 in Figure 8c. The mentioned inter-story drift ratio was obtained from the maximum inter-story drift ratios of three sequence records in CMF1 and CMF2 in every story. The minimum inter-story drift ratios were calculated as much as 7.44E-04 and

2.92E-04 at the first level of CMF1 and CMF2, respectively. Moreover, some fluctuations resulted in the maximum mentioned parameters reaching 3.43E-03 and 1.67E-03 at the seven and 24 levels of CMF1 and CMF2, respectively.

Figure 9 shows the maximum drifts of CMF1 and CMF2 subjected to sequence records. There were substantial differences in the proportion of maximum drifts of CMF1 and CMF2 at different levels. CMF1 drifted 3.43E-03 at the Combinedsery1 record, whereas CMF2 drifted only 1.67E-03 at the Combinedsery1 record. In addition, the least maximum drift difference is at the Combinedsery3 record, where 1.26E-03 was obtained for CMF1 compared with the 7.76E-04 drift of CMF2. Combinedsery3 records a larger maximum drift inter-story for CMF1 than for CMF2 (2.34E-03, 1.28E-03).

Figure 9 demonstrates the maximum inter-story drift under the Combinedsery1 record at 24 levels of CMF2. According to maximum inter-story drift in 24 floors in CMF2, figure 10a illustrates the nonlinear time history analysis of drift based on the X and Y directions for the combinedsery1 record in 24 levels. The SPSS software was used to analyze the data and provided more accurate information in Figure 10a. Significant differences were observed proportional to CMF1 and CMF2 at box plots outputs. Additionally, some data in the top and bottom of the box plot in Figure 10b related to CMF1 as the scattered data. CMF2 had less scattered data at the top and bottom of the box plot in Fig 10c than CMF1.

Furthermore, the CMf2 box plot showed a lower domain, as much as -0.002 and 0.002, than CMF1 by more domains in -0.003 and 0.003. Hence, the data concentration in CMF2 at the X-direction was more than

in CMF1. Furthermore, the CMF2 box plot by -0.001 and 0.001 range indicated a lower domain than CMF1 by domains in -0.002 and 0.002 in the Y direction in Figure 10d-e.

Consequently, the data behavior in CMF2 presented more concentration than that in CMF1 by statistical studies. The appropriate performance of the end shear walls increases confinement.

In the following, the normal Q-Q plots were discussed for further investigation of 24 levels of CMF1 and CMF2 structures subjected to Combinedsery1 records (Figure 11). According to the normal Q-Q plot of XCMF1 in Figure 11a, the excepted normal in the vertical axis was at -5.0 and 5.0 of the domain. Additionally, the horizontal axis showed a range between -0.003 and 0.003. A normal Q-Q plot of XCMF2 in Figure 11b showed the excepted normal from -4 to 4, and the observed values ranged from -0.002 to 0.002. The XCMF2 data were much closer to the line than the XCMF1 data.

In Figure 11c, the normal Q-Q plot for YCMF1 shows an excepted normal range of -5 to 5 and an observed value domain of -0.002 to 0.002. In addition, the mentioned domains of YCMF2 were observed from -4 to 4 and -0.001 to 0.001 in Figure 11d, respectively. Also, most of the YCMF2 data is located on line in Figure 11d.

Figure 12 shows the frequency histogram for 24 levels of CMF2 and CMF1 structures under combinedsery1. The frequency of CMF1 in the X direction in Combinedsery1 is presented in Figure 11a. The data frequency was observed between 3000 to 4000, with the standard deviation and mean of 5.948E-4 and 1.52E-5, respectively. Based on the data domain, the data ranges were from -0.003 to 0.003. On the other hand, the frequency domain ranged from 1500 to 2000 with the standard deviation and mean of 3.158E-4 and -2.23E-6 by accumulating XCMF2 data in Figure 11b. In addition, the frequency of CMF1 in the Y direction in Combinedsery1 ranged from 3000 to 4000 in Figure 11c. The standard deviation and mean were as much as 4.732E-4 and 1.21E-5, respectively. The data domain of the horizontal graph mentioned was from -0.002 to 0.002 in Figure 11c. The frequency of CMF2 in the Y direction of Combinedsery1 is presented in Figure 11d. The data accumulation was more than in Figure 11c, and the frequency values were from 1000 to 1200, with the standard deviation and mean of 2.502E-4 and 5.95E-6, respectively.

Table 5 illustrates the data statistics outputs of X and Y directions drifts in CMF1 and CMF2 structures in combinedsery1 by SPSS software. The kurtosis and skewness coefficients were significantly lower and closer to zero in CMF2 compared to CMF1 in both directions. The kurtosis coefficient of X-direction drifts of Combinedsery1 in CMF1 significantly dropped from 3.579 to 1.361 compared with CMF2. In addition, the kurtosis coefficient decreased from the Y-direction drift of Combinedsery1 CMF1 (YCMF1) to CMF2 (YCMF2) (4.343 to 0.363). XCMF1 and XCMF2 recorded a skewness coefficient difference of 0.187 and -0.183, respectively.

Moreover, the skewness coefficient changed from 0.143 to 0.051 in YCMF1 and YCMF2, respectively. Then, the sig parameter was calculated in zero outputs for all kurtosis coefficient values. The kurtosis coefficients were significant due to sig parameter values obtained less than 0.05 in Table 5. Descriptive statistics of drifts in the X direction vs. Y direction of Combinedsery1 for CMF1 and CMF2.

The kurtosis and skewness coefficient values under excitation indicated that CMF2 drift data was less dispersed than CMF1.

4. Conclusion

The nonlinear time history analysis is one of the essential analytical methods in tall buildings. This study analyzed two 30-story reinforced concrete structures with and without end shear walls for section properties. The structures were simulated and subjected to three sequences of far-field records by nonlinear time history analysis. The 3D simulation verification of the 30-story structures showed acceptable ratios. The structures were subjected to three sequence records, including Combinedsery1, Combinedsery2, Combinedsery3, and the mentioned records were generated by three far fault records of Northwest China, Morgan Hill, and Loma Prieta. The nonlinear time history analysis data showed that the end shear walls improved structural behavior. Thus, the advantages of an end shear wall can be summarized as follows:

1- Considering some fluctuations in the Combinedsery1 record, the maximum drift decreased by 51% in 30 stories with end shear walls.

2- The results indicated the excepted normal drifts in -5.0 and 5.0 domains in 30 stories without end shear walls structure. In this regard, the normal Q-Q plot showed the excepted normal in -4 and 4 domains for CMF2 in X and Y directions. Thus, the end shear wall declined as much as 20% in the domain of excepted normal in Q-Q plots.

3- In 30 stories without and with end shear walls in the X direction, the frequency domain of drifts decreased from 3000 to 4000 to 1500 to 2000. In addition, the mentioned domains were observed from 3000 to 4000 to 1000 to 1200 in the Y direction. Hence, there was a 50% reduction in data frequency in 30 stories by the end shear wall.

4- The results indicated that the absolute mean of drift data decreased by 85 and 50% in X and Y directions in 30 stories with the end shear wall.

5- The significant structural efficiency of the end shear walls increased in tall buildings. The drift ratio graph in the X direction vs. Y direction showed the maximum reduction of drift ratio at 24 levels of both structures under the Combinedsery1 record. According to these data:

-The graph of drifts related to the 30-story structure with end shear walls experienced a significant drop of kurtosis coefficient by 61% and 92% in the X and Y directions, respectively. The dispersion of drift data for 30-story structures with end shear walls was lower than those without end shear walls.

- As a result of end shear walls, the skewness coefficient of a 30-story building was reduced by 2 and 64%, respectively, in the X and Y directions.

- There was a 47% decrease in standard deviation in both the X and Y directions of the 30-story structure with end shear walls.

Based on the results, the end shear wall outperforms the behavior of the structure under the sequences records of the far field and improves the seismic behavior.

References

1. Shen, J., Ren, X., Zhang, Y., et al. Nonlinear dynamic analysis of frame-core tube building under seismic sequential ground motions by a supercomputer. *Soil Dyn Earthq Eng* [Internet]. 124, pp. 86–97 (2019).

Available from: https://www.sciencedirect.com/science/article/pii/S0267726119302763.

2. Jamnani, HH, Amiri, J.V., Rajabnejad, H. Energy distribution in RC shear wall-frame structures subject to repeated earthquakes. *Soil Dyn Earthq Eng*. 107, pp. 116–28 (2018).

3. Wang, X., Wen, W, Zhai C. Vulnerability assessment of a high- rise building subjected to mainshock–aftershock sequences. *Struct Des Tall Spec Build*. **29**(15), pp. 1786 (2020).

4. Mahmoud, S., Saleem, M., Hasanain, M., et al. Structural response and damage evaluation of a typical highrise RC building in Dubai under an earthquake with single and multiple peaks. *J Civ Eng Manag*. **28**(7), pp. 509–22 (2022).

5. Akhavan Salmassi, M., Kheyroddin, A., Hemmati, A. Seismic behavior of end walls in RC tall buildings with torsional irregularity. *Mag Civ Eng*. 24; pp. 97:9707 (2020).

6. Shokrabadi, M., Burton, H.V. Risk-based assessment of aftershock and mainshock-aftershock seismic performance of reinforced concrete frames. *Struct Saf*. 73, pp. 64–74 (2018).

7. Wen, W., Zhai, C., Ji, D., et al. Framework for the vulnerability assessment of structure under mainshock-aftershock sequences. *Soil Dyn Earthq Eng* [Internet]. 101, pp. 41–52 (2017). Available from: https://www.sciencedirect.com/science/article/pii/S0267726116306327.

8. Zhou, Z., Xu, H., Gardoni, P., et al. Probabilistic demand models and fragilities for reinforced concrete frame structures subject to mainshock-aftershock sequences. *Eng Struct* [Internet]. 245, pp. 112904 (2021). Available from: https://www.sciencedirect.com/science/article/pii/S014102962101052X.

9. Wang, X., Zhang, X., Shahzad, M.M., et al. Fragility analysis and collapse margin capacity assessment of mega-sub controlled structure system under the excitation of mainshock-aftershock sequence. *J Build Eng* [Internet]. 49, pp. 104080 (2022). Available from: https://www.sciencedirect.com/science/article/pii/S2352710222000936.

10. Zhang, Y., Burton, H.V., Shokrabadi, M,et al. Seismic risk assessment of a 42-story reinforced concrete dual-system building considering mainshock and aftershock hazard. *J Struct Eng*. **145**(11), pp. 4019135 (2019).

11. Zhang, Y., Burton, H.V. Optimal decision-making for tall buildings in the aftershock environment. *Autom Constr* [Internet]. 122, pp. 103472. Available from: https://www.sciencedirect.com/science/article/pii/S0926580520310529.

12. Huang, W., Shi, F., Zhang, C., et al. Seismic performance of reinforced concrete frame with lead viscoelastic damper under mainshock-aftershock sequences. Structures [Internet]. 41, pp. 1624–36 (2022). Available from: https://www.sciencedirect.com/science/article/pii/S2352012422004684.

13. Zhang, Y., Burton, H.V. Pattern recognition approach to assess the residual structural capacity of damaged tall buildings. *Struct Saf* [Internet]. 78, pp. 12–22 (2019). Available from: https://www.sciencedirect.com/science/article/pii/S0167473018301334.

14. Tesfamariam, S., Goda, K. Energy-Based Seismic Risk Evaluation of Tall Reinforced Concrete Building in Vancouver, BC, Canada, under M w9 Megathrust Subduction Earthquakes and Aftershocks. *Front Built Environ*. 3, pp.29 (2020).

15. Mantawy, A., Anderson, J.C. Earthquake damage potential due to low-cycle fatigue in RC moment frame buildings. In: *Tenth US National Conference on Earthquake Engineering Frontiers of Earthquake Engineering July*. pp. 5–21 (2014).

16. Maharjan, P. Seismic Fragility Assessment of Rc Frame Structures Under Main Shock-Aftershock Sequences Using Incremental Dynamic Analysis. Pulchowk Campus, (2021).

17. Tsai, K.C., Hsiao, C.P., Bruneau, M. Overview of building damages in 921 Chi-Chi earthquakes. *Earthq Eng Eng Seismol.* **2**(1), pp. 93–108 (2000).

18. Tauheed, A., Alam, M., Datta, T.K. Performance of RC Frames with Stiffness Irregularity Under Sequential Ground Motion. In: *Recent Advances in Structural Engineering*. Springer, pp. 145–54 (2021).

19. Tauheed, A., Alam, M. Seismic performance of RC frames under sequential ground motion. *Asian J Civ Eng.* **22**(8), pp. 1447–60 (2021).

20. Tauheed, A., Alam, M., Datta, T.K. Influence of mass irregularity on the response of RC frame with stiffness irregularity by non-linear time history analysis. In: *Recent Advances in Earthquake Engineering*. Springer; pp. 135–59 (2022).

21. Naserpour, A., Fathi, M. Numerical study of a multiple post-tensioned rocking wall-frame system for seismic resilient precast concrete buildings. *Earthq Eng Eng Vib*. **21**(2), pp. 377–93 (2022).

22. Abdelnaby, A.E., Elnashai, A.S. Numerical modeling and analysis of RC frames subjected to multiple earthquakes. *Earthquakes Struct.* **9**(5), pp. 957–81 (2015).

23. Han, R., Li, Y., van de Lindt J. Assessment of seismic performance of buildings with the incorporation of aftershocks. *J Perform Constr Facil.* **29**(3), pp. 4014088 (2015).

24. Han, R., Li, Y,, van de Lindt J. Impact of aftershocks and uncertainties on the seismic evaluation of non-ductile reinforced concrete frame buildings. *Eng Struct.* 100, pp. 149–63 (2015).

25. Tahara, R.M.K., Majid, T.A., Zaini, S.S., et al. Effect of the repeated earthquake on inelastic moment resisting concrete frame. In: *AIP Conference Proceedings. AIP Publishing LLC*, pp. 20019 (2017).

26. Rinaldin, G., Amadio, C., Fragiacomo, M. Effects of seismic sequences on structures with hysteretic or damped dissipative behavior. *Soil Dyn Earthq Eng*. 97, pp. 205–15 (2017).

27. Hatzigeorgiou, G.D., Liolios, A.A. Nonlinear behavior of RC frames under repeated strong ground motions. *Soil Dyn Earthq Eng*. **30**(10), pp. 1010–25 (2010).

28. Wang, X.M.M., Shahzad, X. Fragility analysis and collapse margin capacity assessment of mega-sub controlled structure system under the excitation of mainshock-aftershock sequence. *Journal of Building Engineering*. 49, pp. 80-104 (2022).

29. Soureshjani, O.K., Massumi, A. Seismic behavior of RC moment resisting structures with concrete shear wall under mainshock–aftershock seismic sequences. *Bulletin of Earthquake Engineering*. **20**(2), pp. 1087-1114 (2022).

30. Akhavan Salmassi, M., Gerami, M., Heidari Tafreshi, A. Evaluation of Flexible Steel Frame Structures with Post Tensioned Cables to Sequences Far From Fault. *Journal of Structural and Construction Engineering*. **6**(3), pp. 221-234 (2019).

31 . Qiao, Y.M., Lu, D.G., Yu, X.H. Shaking table tests of a reinforced concrete frame subjected to mainshock-aftershock sequences. *Journal of Earthquake Engineering*. **26**(4), pp. 1693-1722 (2022).

32. Liu, J., Tian, L., Meng, X., et al. Seismic fragility assessment of a transmission tower considering mainshock-aftershock sequences. *Journal of Constructional Steel Research*. 194, pp. 107-344 (2022).

33. Bao, X., Jin, L., Liu, J., et al. Framework for the mainshock-aftershock fragility analysis of containment structures incorporating the effect of mainshock-damaged states. *Soil Dynamics and Earthquake Engineering*. 153, pp.72-107 (2022).

34. Wen, W., Ji, D., Zhai, C. Cumulative Damage of Structures under the Mainshock-aftershock Sequences in the Near-fault Reg.ion. *Journal of Earthquake Engineering*. **26**(4), pp. 2088-2102 (2022).

35. Hosseini, S., Naderpour, H., Vahdani, R., et al. Evaluation of pounding effects between reinforced concrete frames subjected to far-field earthquakes in terms of damage index. *Bulletin of Earthquake Engineering*. **20**(2), pp. 1219-1245 (2022).

36. Basim, M.C., Pourreza, F., Mousazadeh, M., et al. The effects of modeling uncertainties on the residual drift of steel structures under mainshock-aftershock sequences in Structures. *Elsevier*. pp. 912-926 (2022).

37. Pu, W., Li, Y. Evaluating structural failure probability during aftershocks based on spatiotemporal simulation of the regional earthquake sequence, *Engineering Structures*. 275, pp. 115267 (2023).

38. Lu, X., Xie, L., Guan, H., et al. A shear wall element for nonlinear seismic analysis of super-tall buildings using OpenSees. *Finite Elem Anal Des*. 98, pp. 14–25 (2015).

39. Parra, P.F., Arteta, C.A., Moehle, J.P. Modeling criteria of the older non-ductile concrete frame–wall buildings. *Bull Earthq Eng* [Internet]. **17**(12), pp. 6591–620 (2019). Available from: https://doi.org/10.1007/s10518-019-

00697-y.

Table 1. The specifications of buildings

Label	Story	H (m)	A (m^2)	Plan Dimensions (m×m)	Story
CMF1- (Without End shear wall)	30	120	36750	35×35	30
CMF2- (With End shear wall)	30	120	36750	35×35	30

Table 2. The specifications of the sections

Label	Dimension	Rebar
Beam	St1-30: (0.5) m wide × (0.7) m deep	8Φ20- Stirrup Φ14@10
Column	St1-15:(1.20) m × (1.20) m, St16-30:(1.00) m × (1.00) m	36Φ32 - 36Φ32 – Stirrup Φ14@15
Shear Wall	St1-30:(35) m long × (0.5) m thick	Φ28@10 - Stirrup Φ14@25
End shear wall	St1-30:(11) m long × (0.5) m thick	Φ28@10 - Stirrup Φ14@25
Slab	St1-30:(0.15) m thick	Φ10@10

Table 3. The specifications of far-field earthquake records.

ID No.	Event	Station	Year	M_w	d (km)	PGA $_{max}$(g)	PGA $_{max}$(g)/ PGV $_{max}$(cm/sec)
R1	Loma Prieta	Gilroy Array #4	1989	6.93	14.34	0.419	1.040
R2	Morgan Hill	Gilory Array #4	1984	6.19	11.54	0.349	2.010
R3	Northwest China-03	Jaishi	1997	6.1	17.73	0.3	1.558

Table 4. Verification results.

Analysis type	maximum base shear/W (%)
Article analysis	10.5
Verification analysis	11.1

Table 5. Descriptive statistics of drifts in the X direction vs. Y direction of Combinedsery1 for CMF1 and CMF2.

	N	Std. Deviation	Skewness	Kurtosis

	Statistic	Statistic	Statistic	Std. Error	Statistic	Std. Error
XCMF1	24023	.00059	0.187	0.016	3.579	0.032
YCMF1	24023	.00047	0.143	0.016	4.343	0.032
XCMF2	24020	.00032	-0.183	0.016	1.361	0.032
YCMF2	24020	.00025	0.051	0.016	0.363	0.032
Valid N (listwise)	24020					

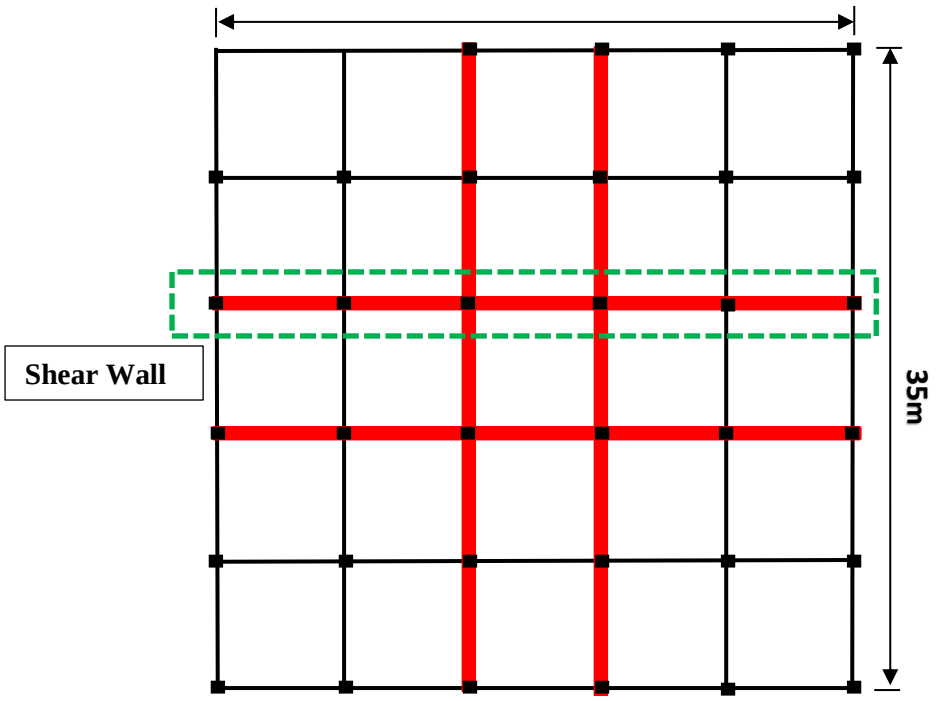

(a) The typical floor plan of structure without end shear wall

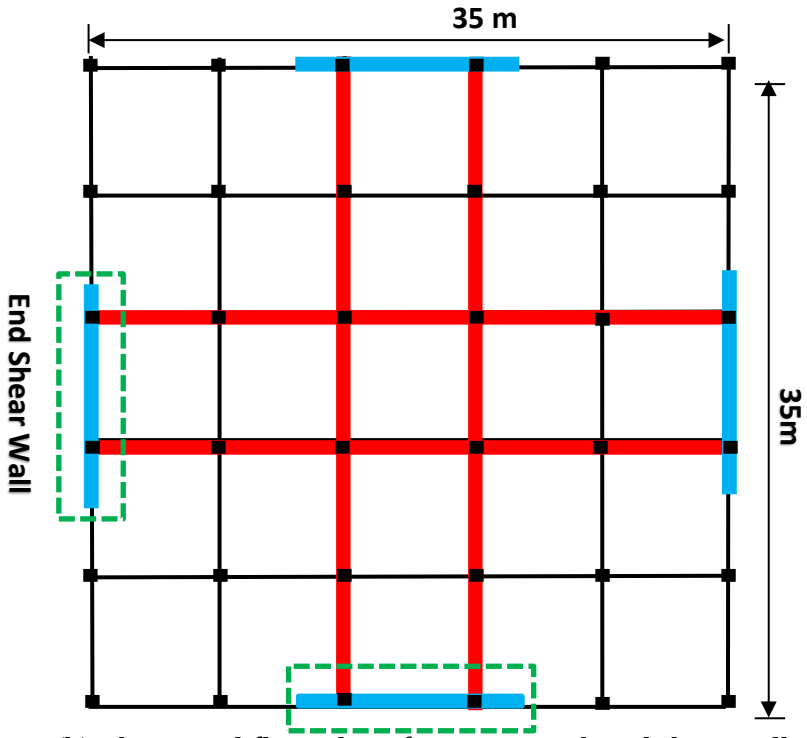

(b) The typical floor plan of structure with end shear wall

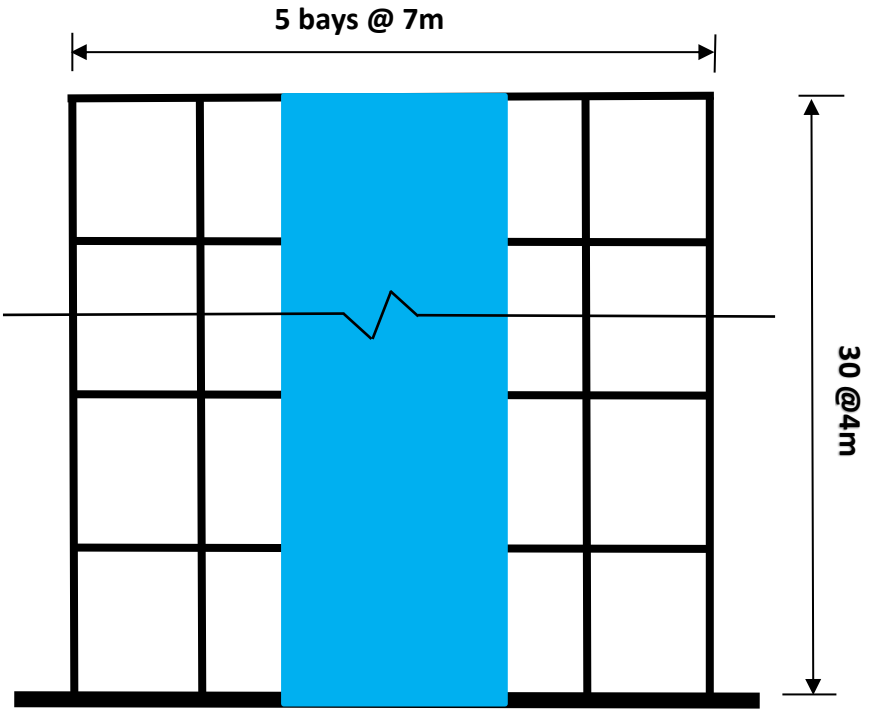

(c) The typical frame elevation of structure with end shear wall

Figure 1. The 30-story model

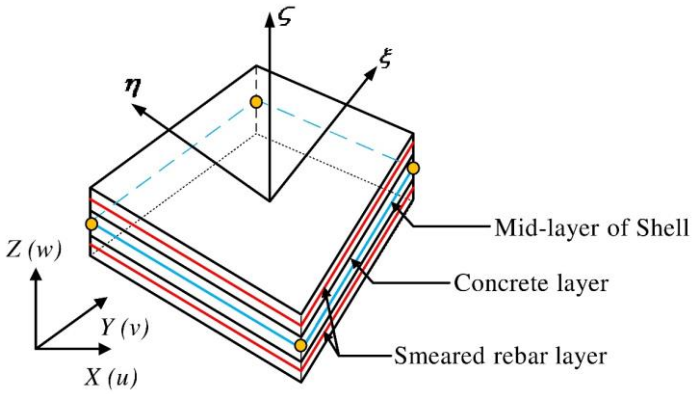

Figure 2. Multi-layer shell element [39].

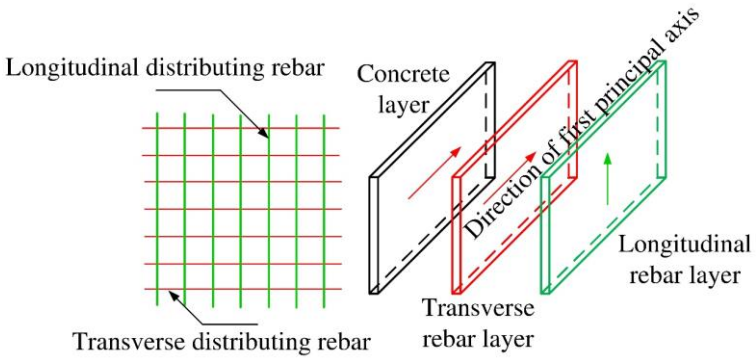

Figure 3. Distribution of rebar layer [39].

459

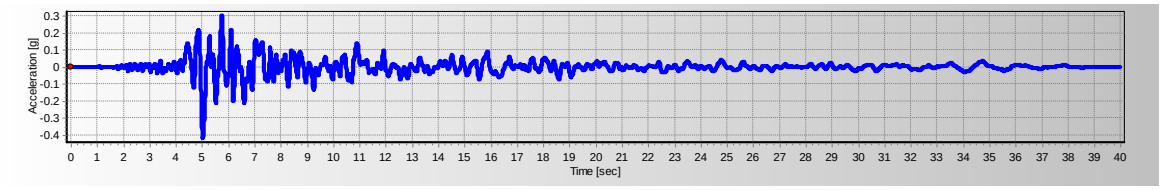

(a) Loma Prieta, acceleration-time.

(b) Loma Prieta, response acceleration-time.

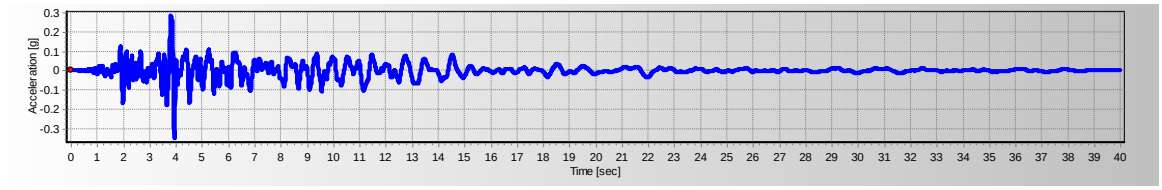

(c) Morgan Hill, acceleration-time.

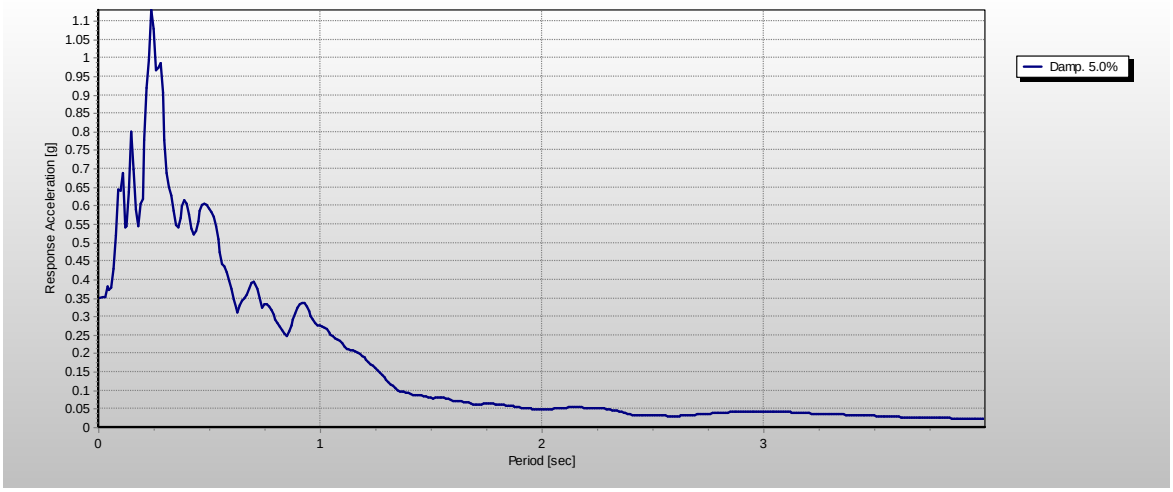

(d) Morgan Hill, response acceleration-time.

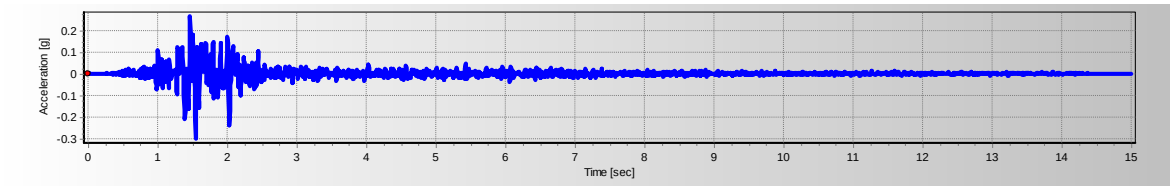

(e) Northwest china-03, acceleration-time.

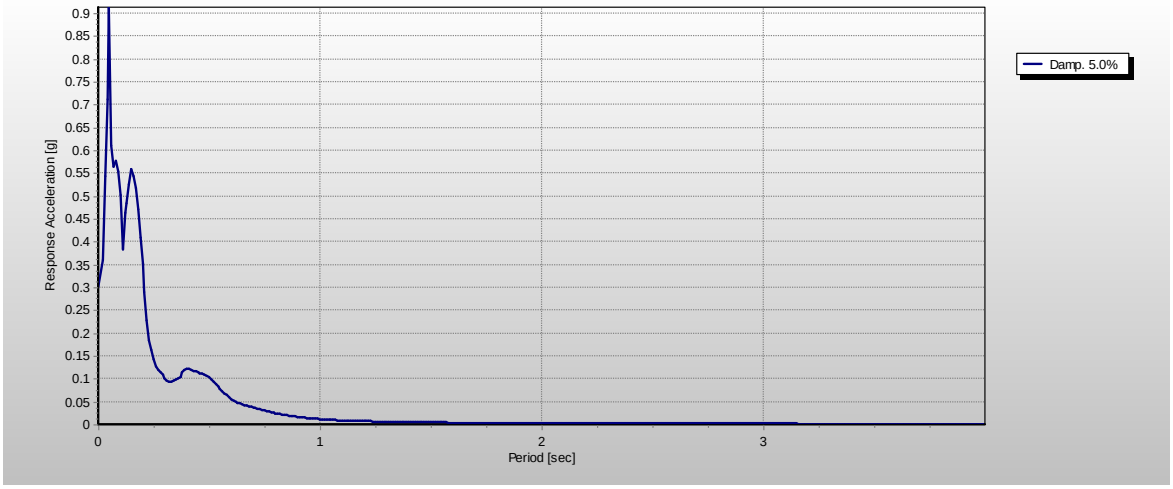

(f) Northwest china-03, response acceleration-time.

Figure 4. The acceleration-time and response acceleration-time graphs of records.

460

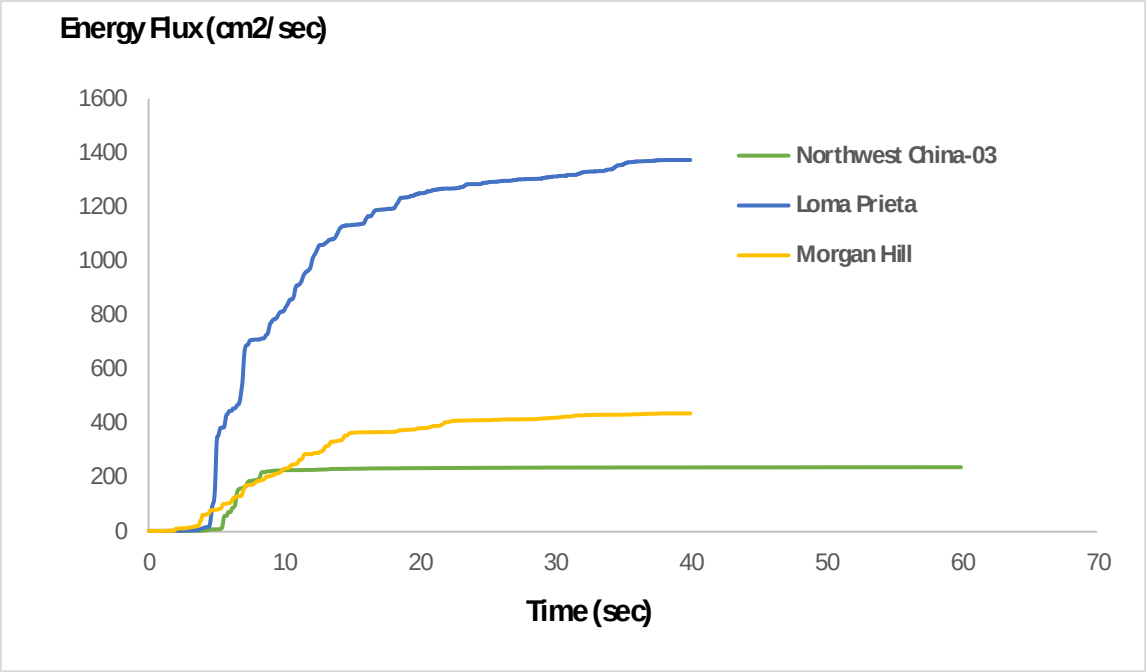

Figure 5. The energy flux-time graphs of records.

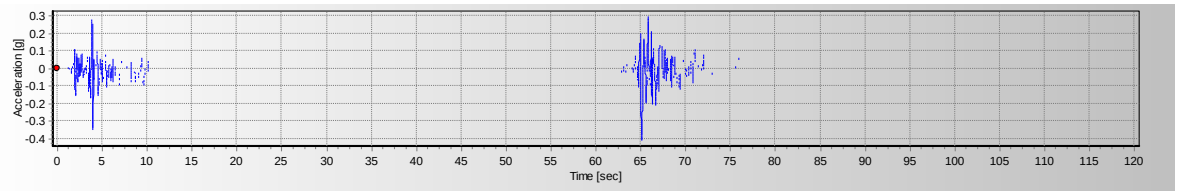

Combinedsery1

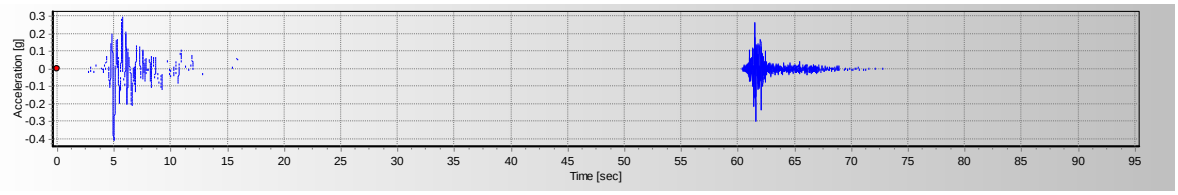

Combinedsery2

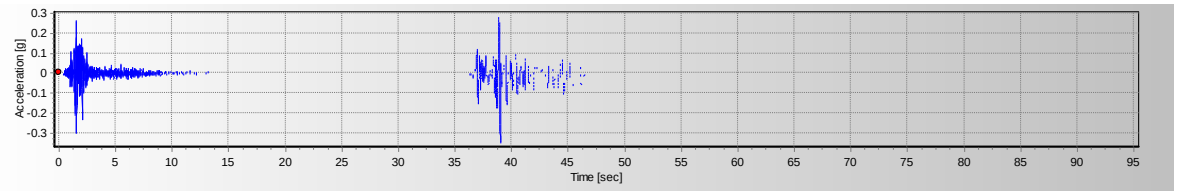

Combinedsery3

Figure 6. The acceleration-time graphs of sequence records.

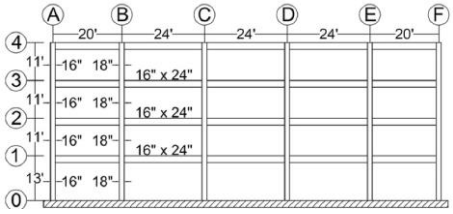

(a) The detail of Parra et al. (2019) frame [39].

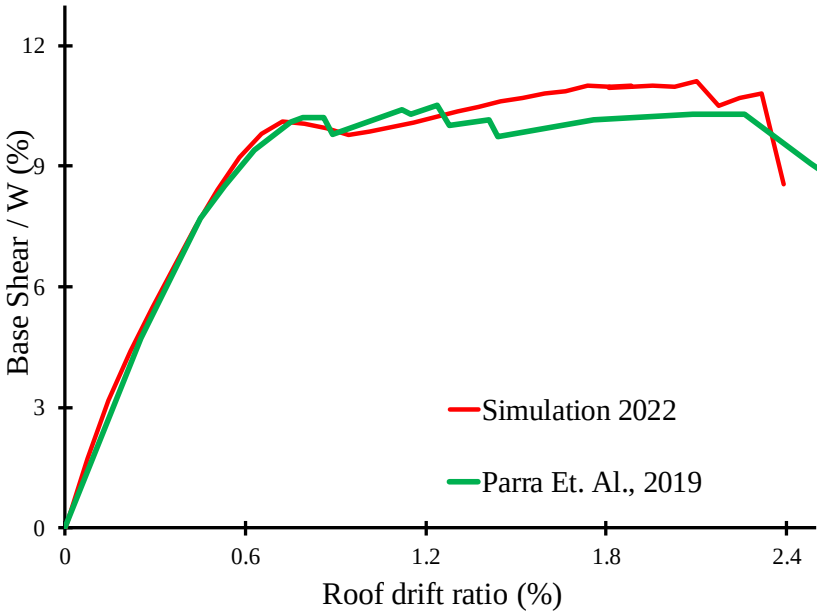

(b) Base shear/W (%) – roof drift ratio (%) graphs.

Figure 7. The verification detail of the frame.

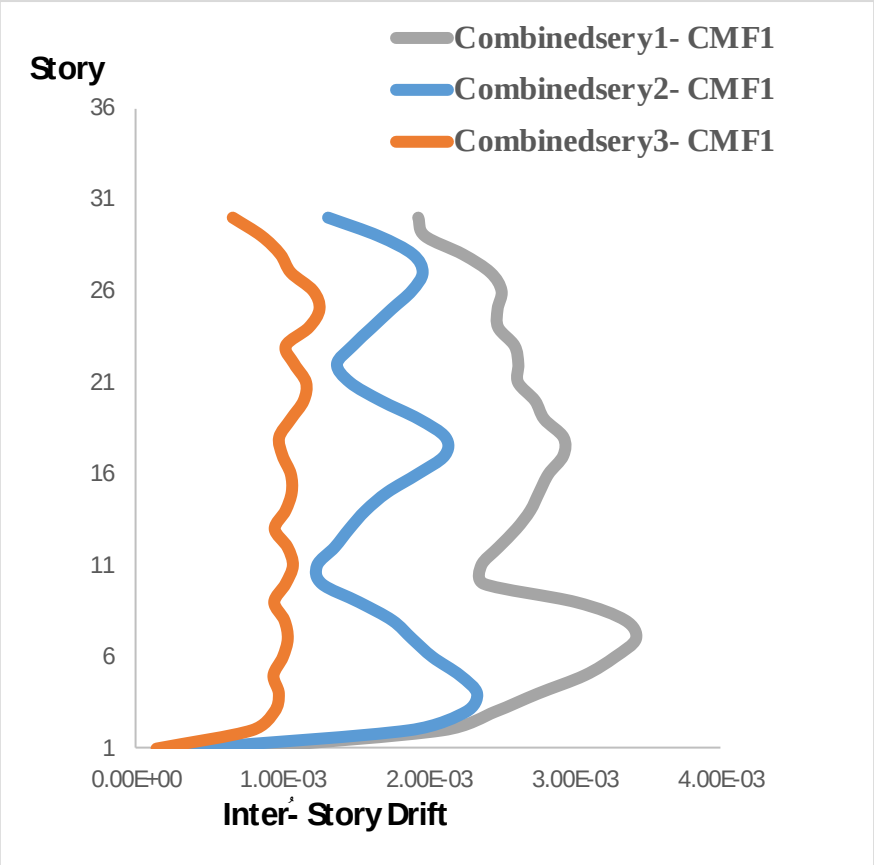

(a) Inter-story drift ratio-story CMF1.

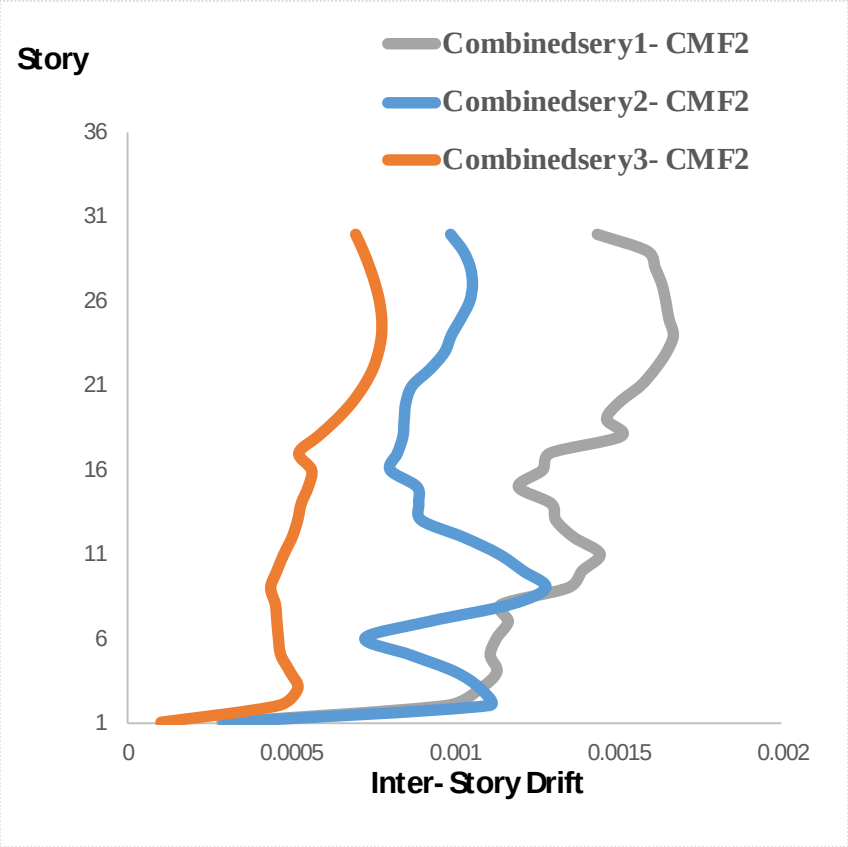

(b) Inter-story drift ratio-story CMF2.

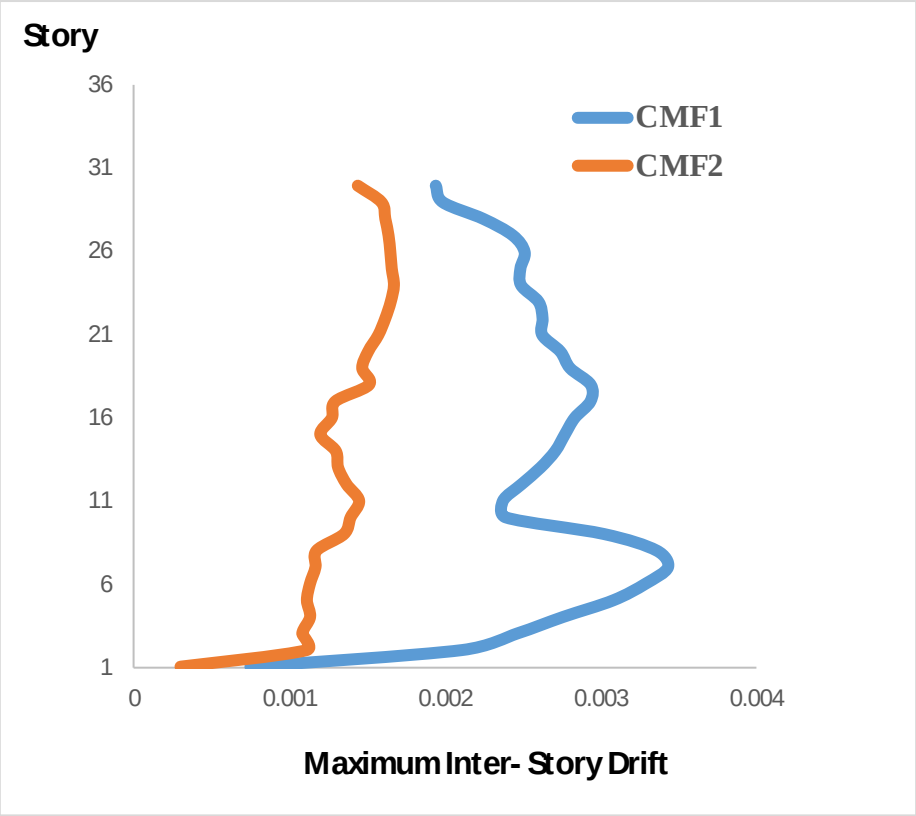

(c) Maximum inter-story drift ratio-story CMF1 and CMF2.
Figure 8. The inter-story drift ratio-story.

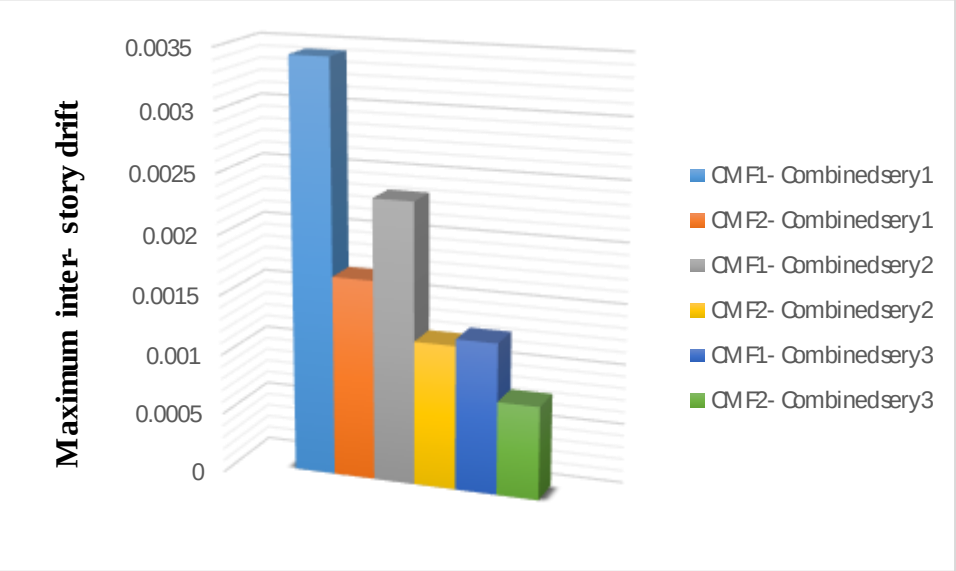

Figure 9. The comparison of the maximum inter-story drift values in sequence records.

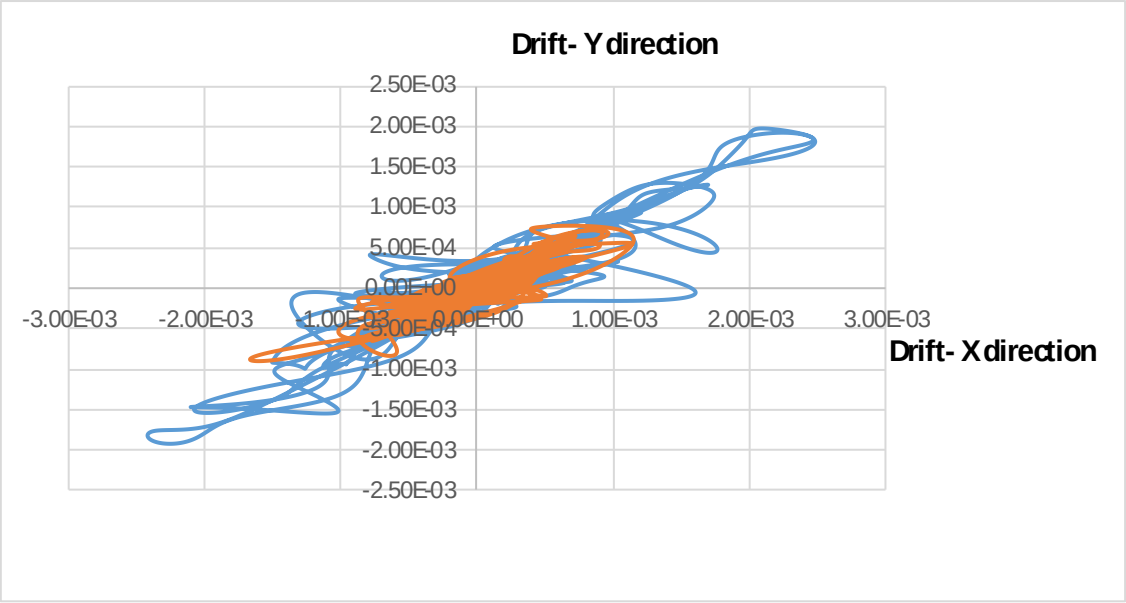

(a) The drift in the X direction vs. Y direction of CMF1 and CMF2 under Combinedsery1.

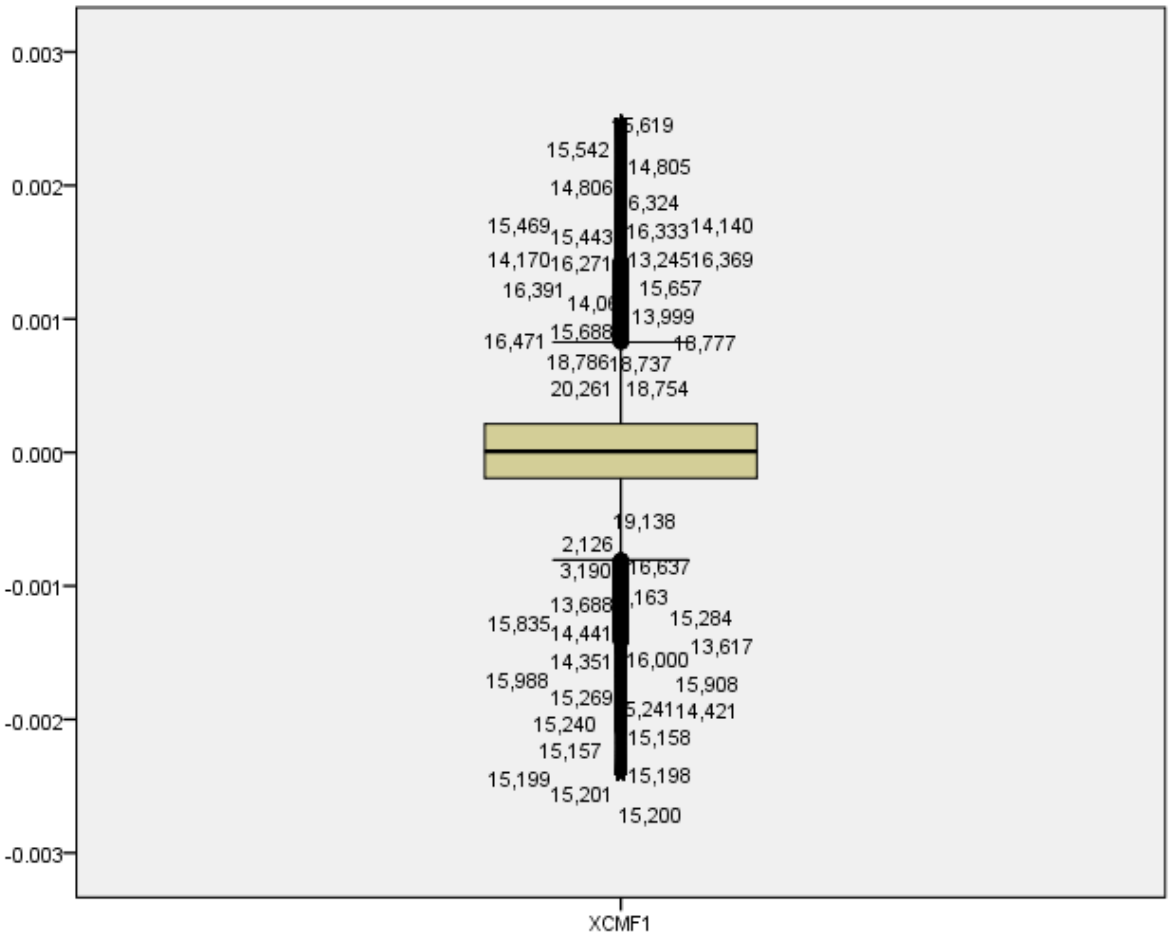

(b) The Box plot of drift in the X direction of CMF1 in Combinedsery1.

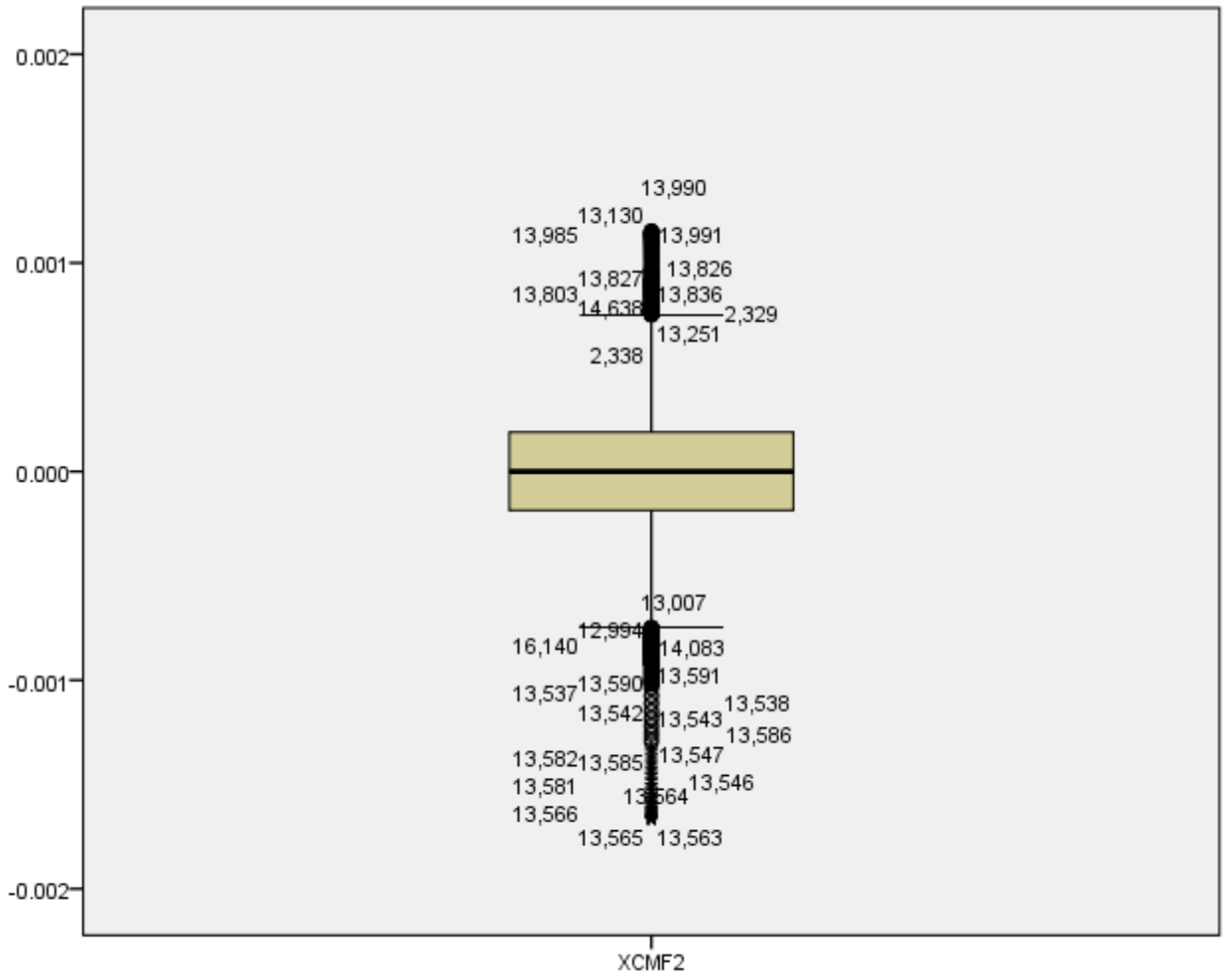

(c) The Box plot of drift in the X direction of CMF2 in Combinedsery1.

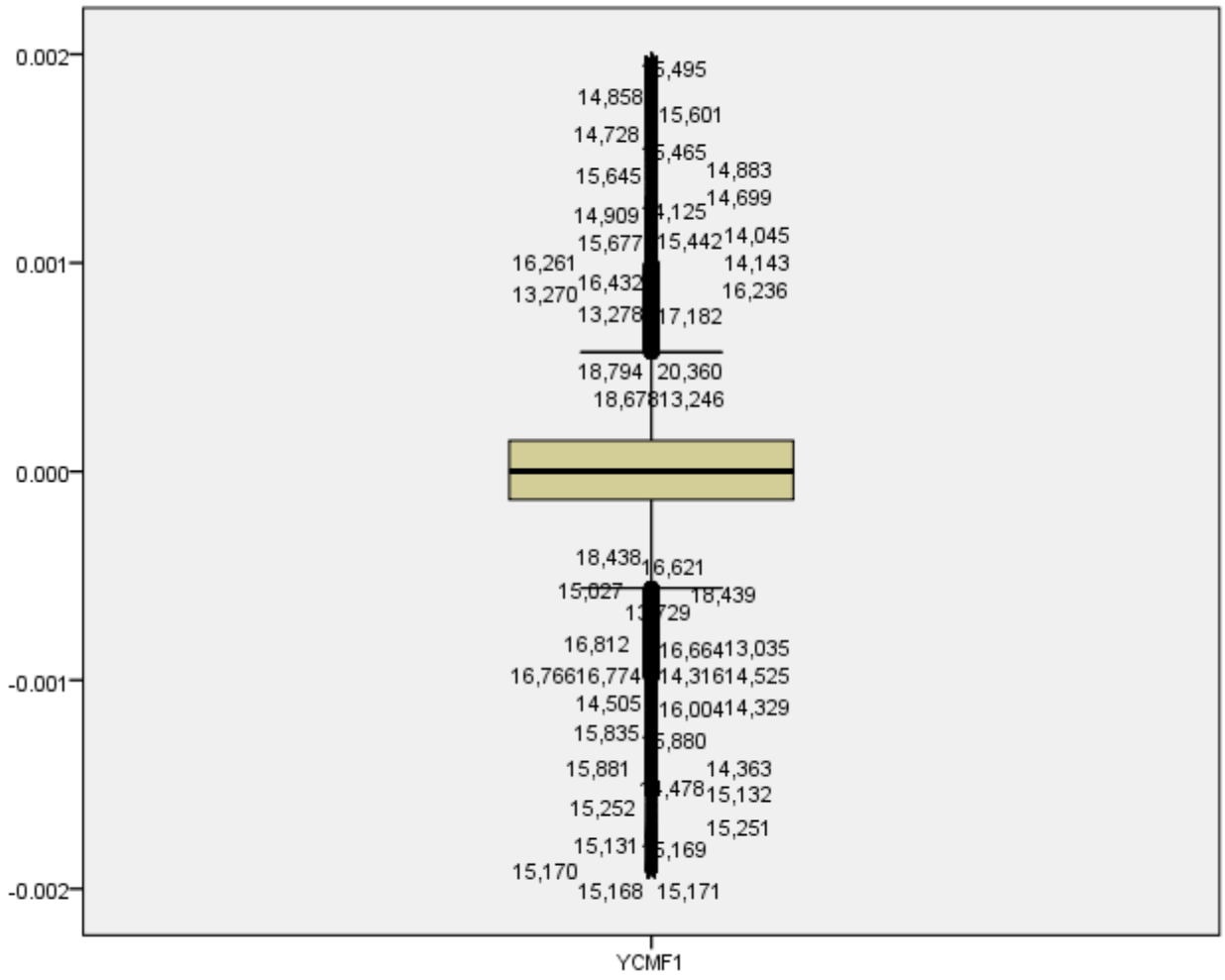

(d) The Box plot of drift in the Y direction of CMF1 in Combinedsery1.

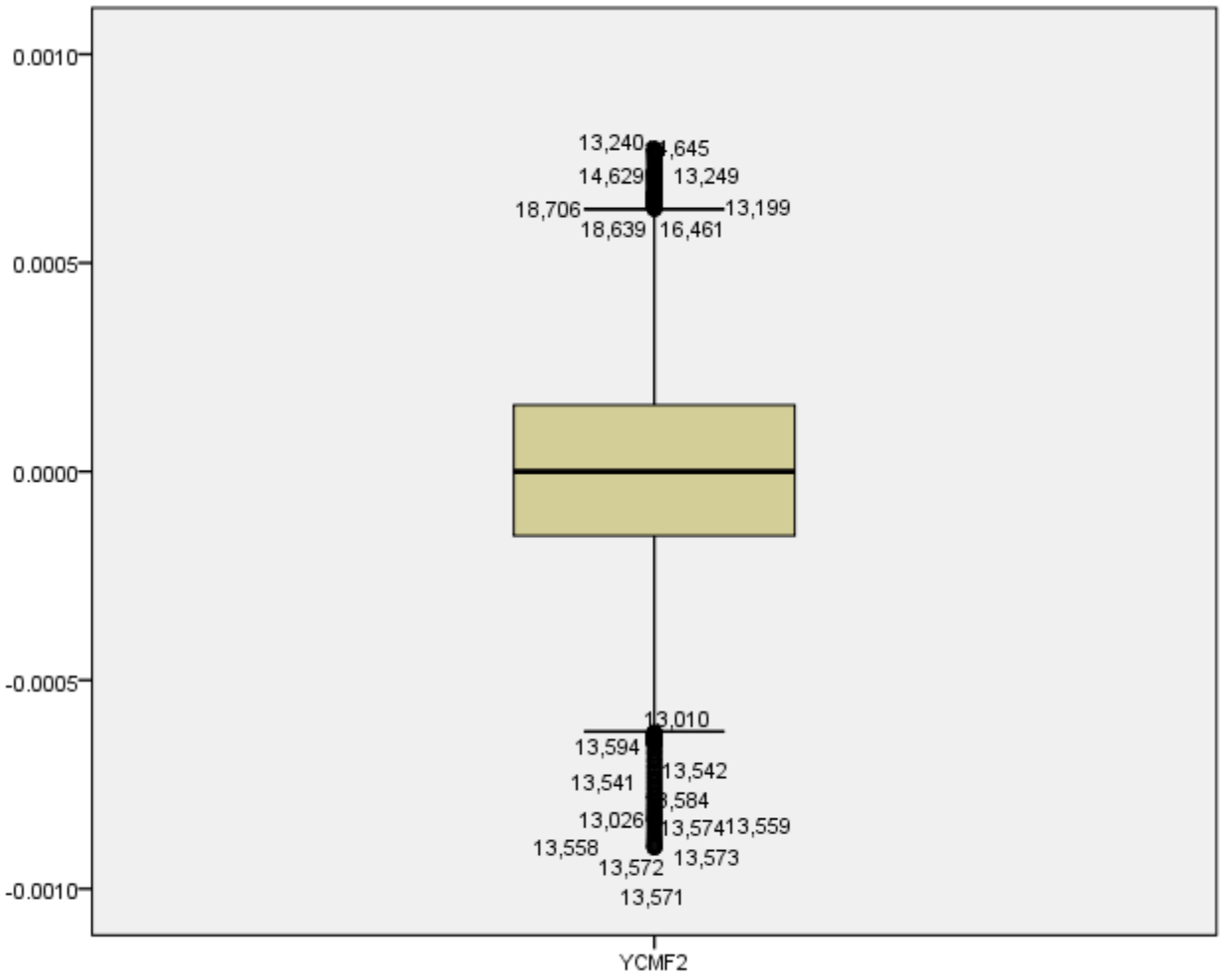

(e) The Box plot of drift in the Y direction of CMF2 in Combinedsery1.

Figure 10. The drifts and box plots of CMF1 and CMF2 in the X and Y directions in Combinedsery1.

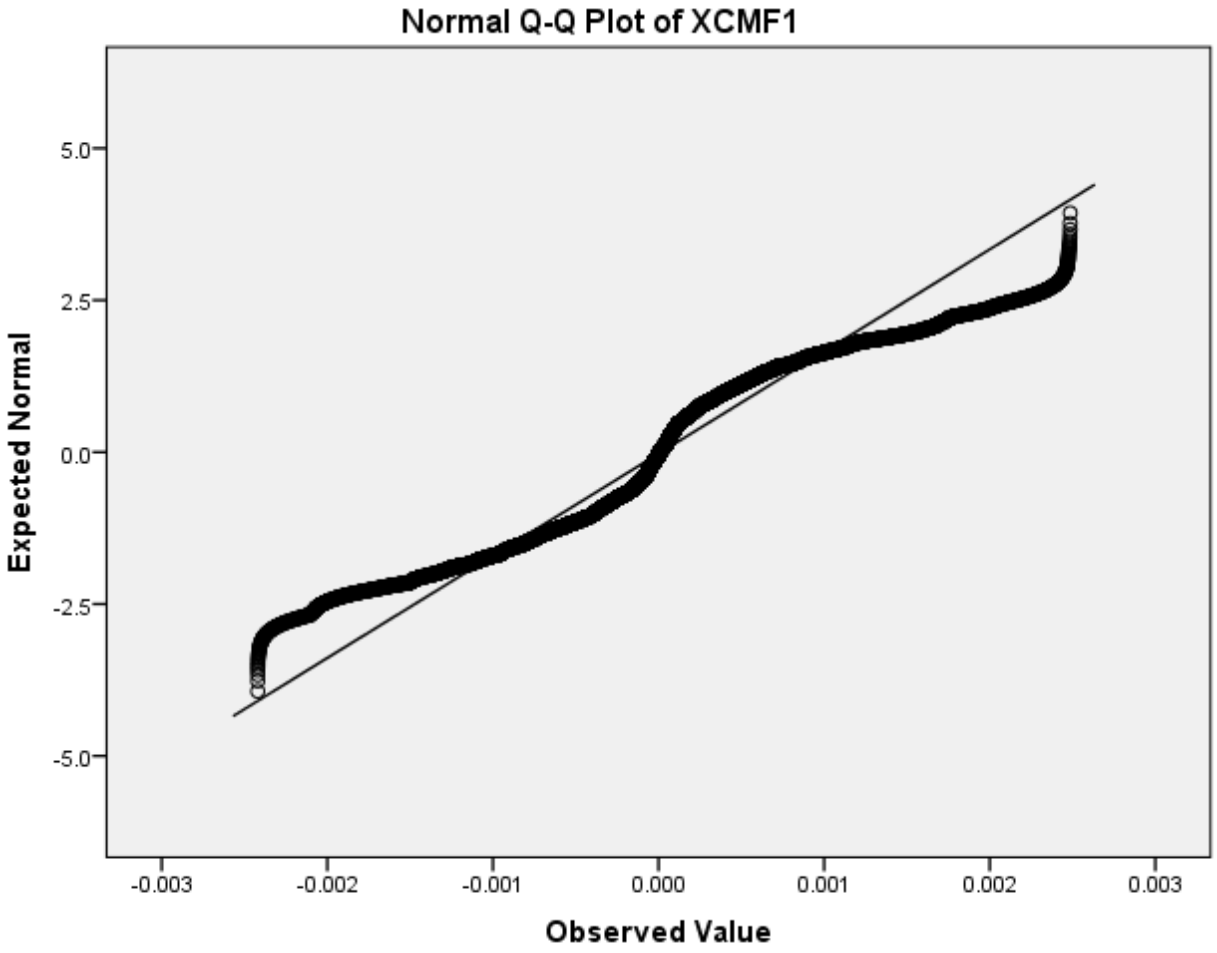

(a) The Normal Q-Q plots of CMF1 in the X direction in Combinedsery1.

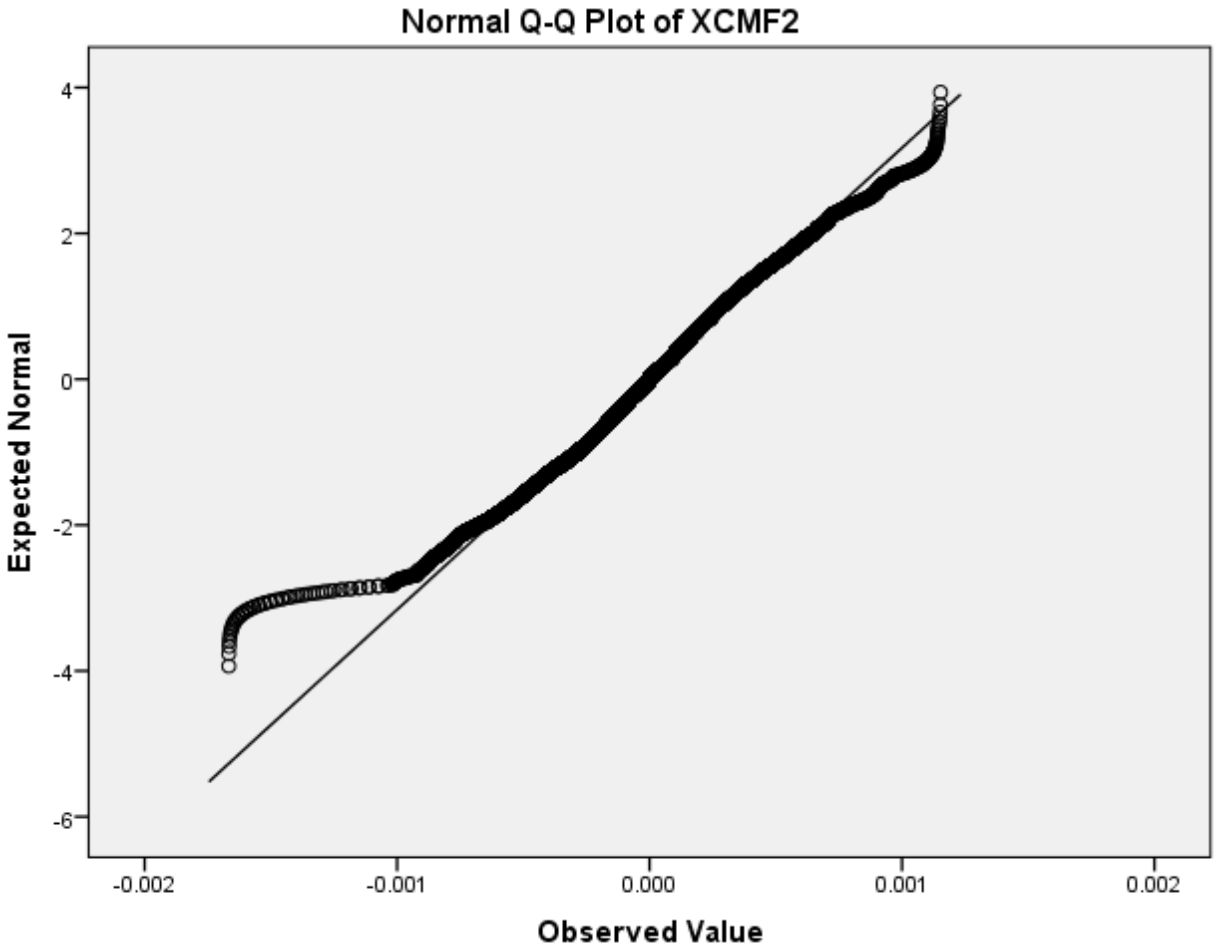

(b) The Normal Q-Q plots of CMF2 in the X direction in Combinedsery1.

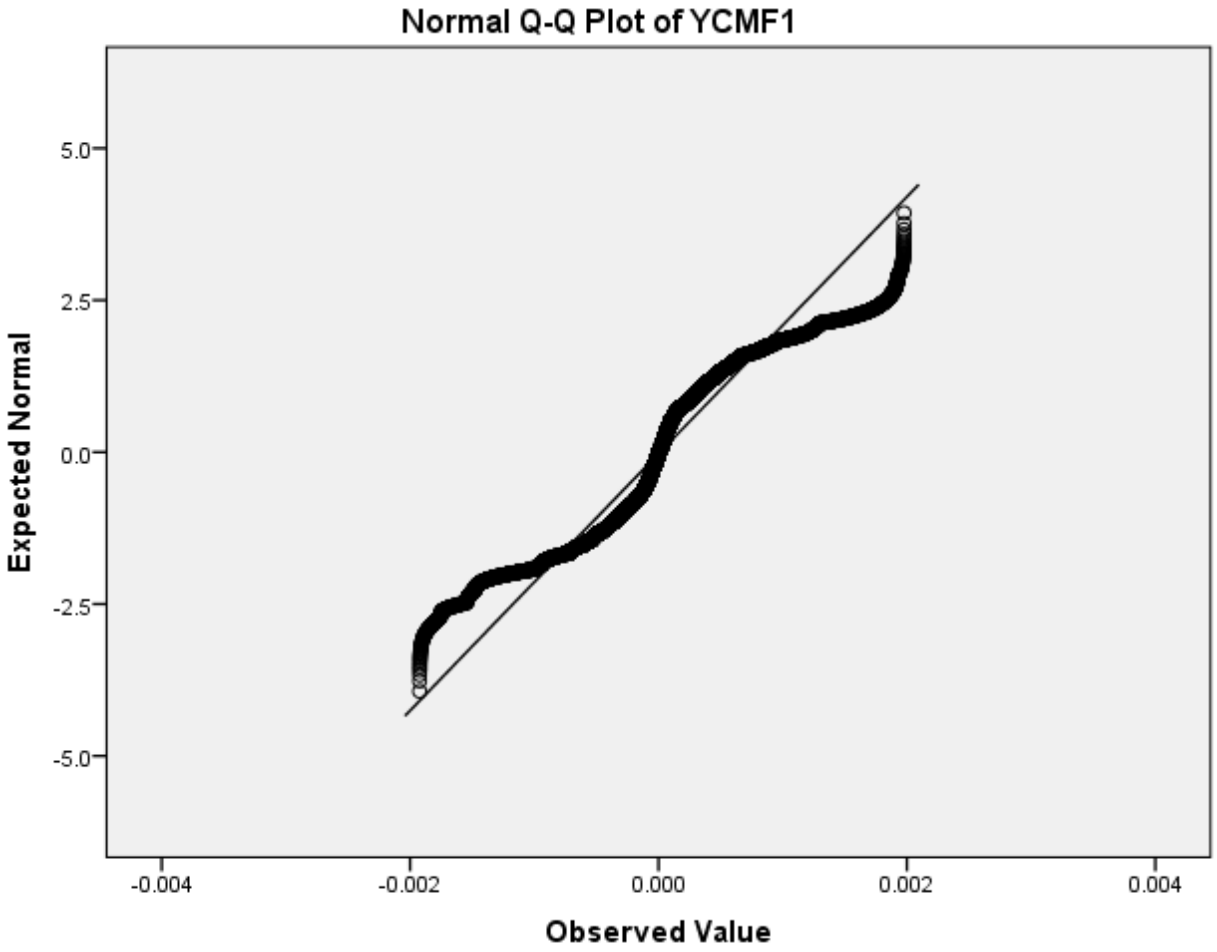

(c) The Normal Q-Q plots of CMF1 in the Y direction in Combinedsery1.

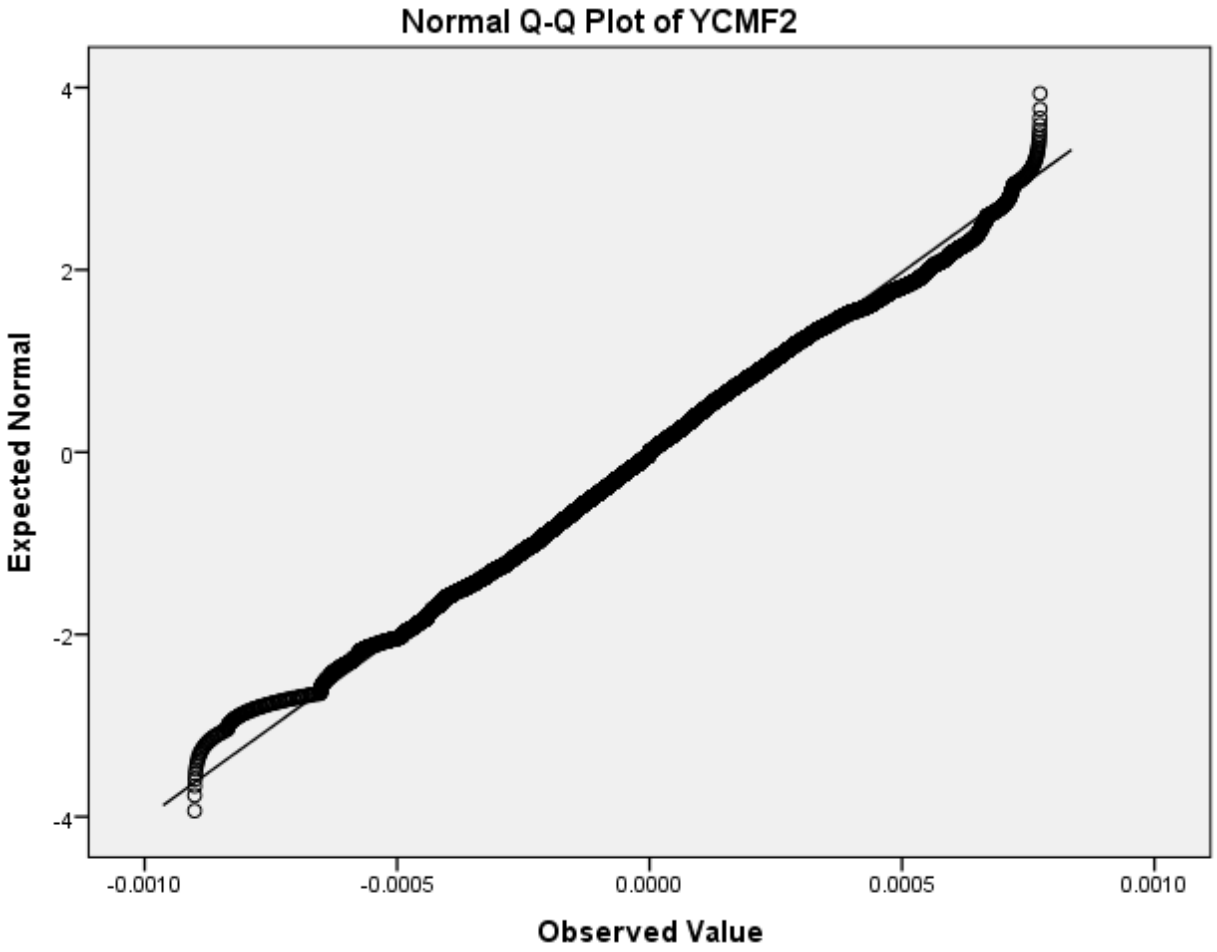

(d) The Normal Q-Q plots of CMF2 in the Y direction in Combinedsery1.

Figure 11. The Q-Q plots of CMF1 and CMF2 in X and Y directions in Combinedsery1.

480

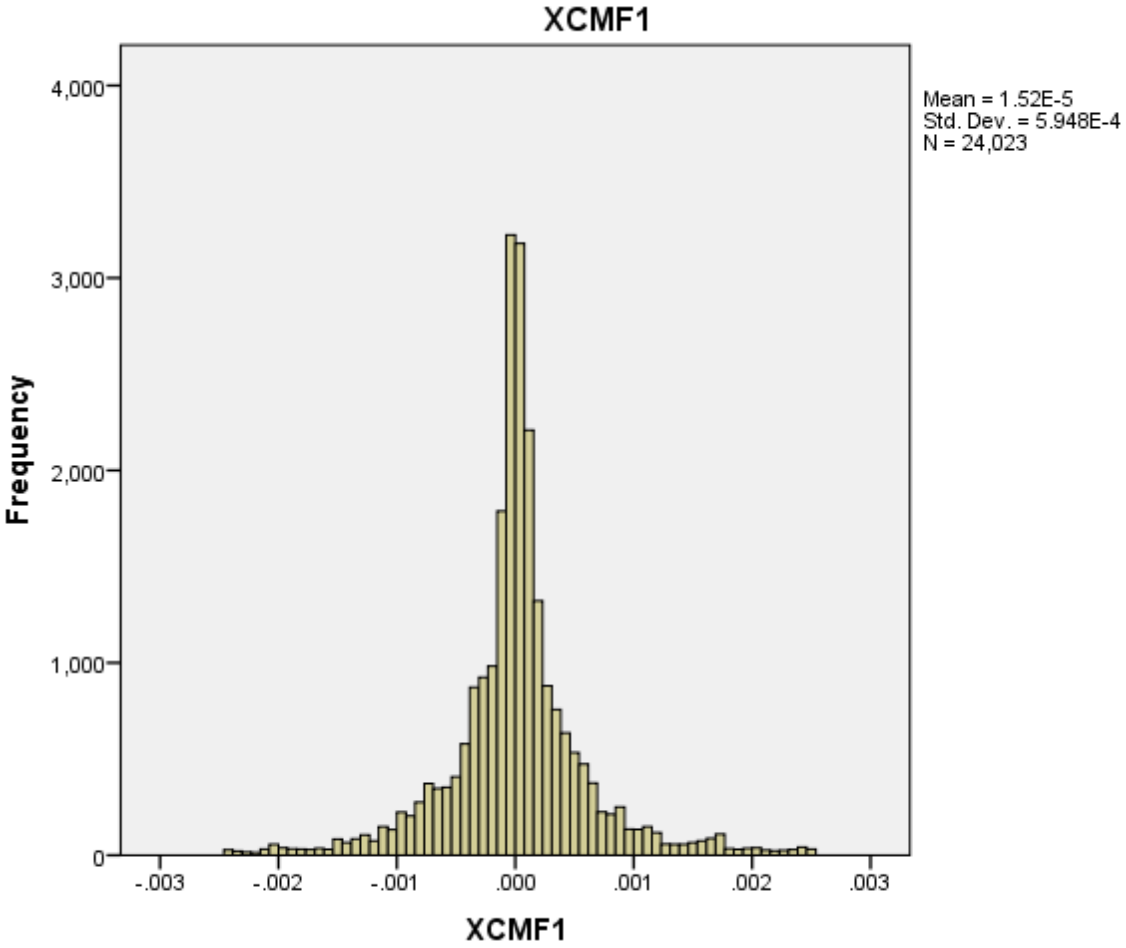

(a). The frequency of CMF1 in the X direction in Combinedsery1.

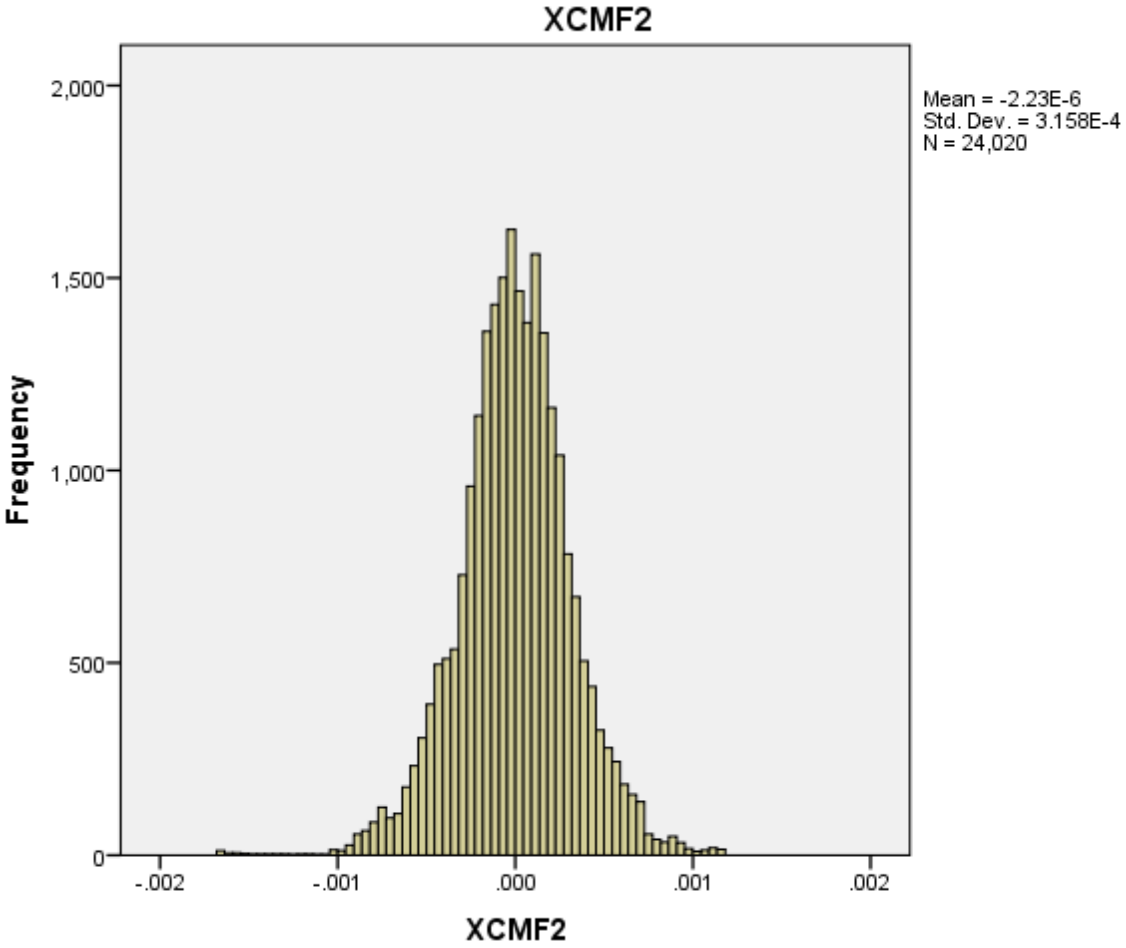

(b) The frequency of CMF2 in the X direction in Combinedsery1.

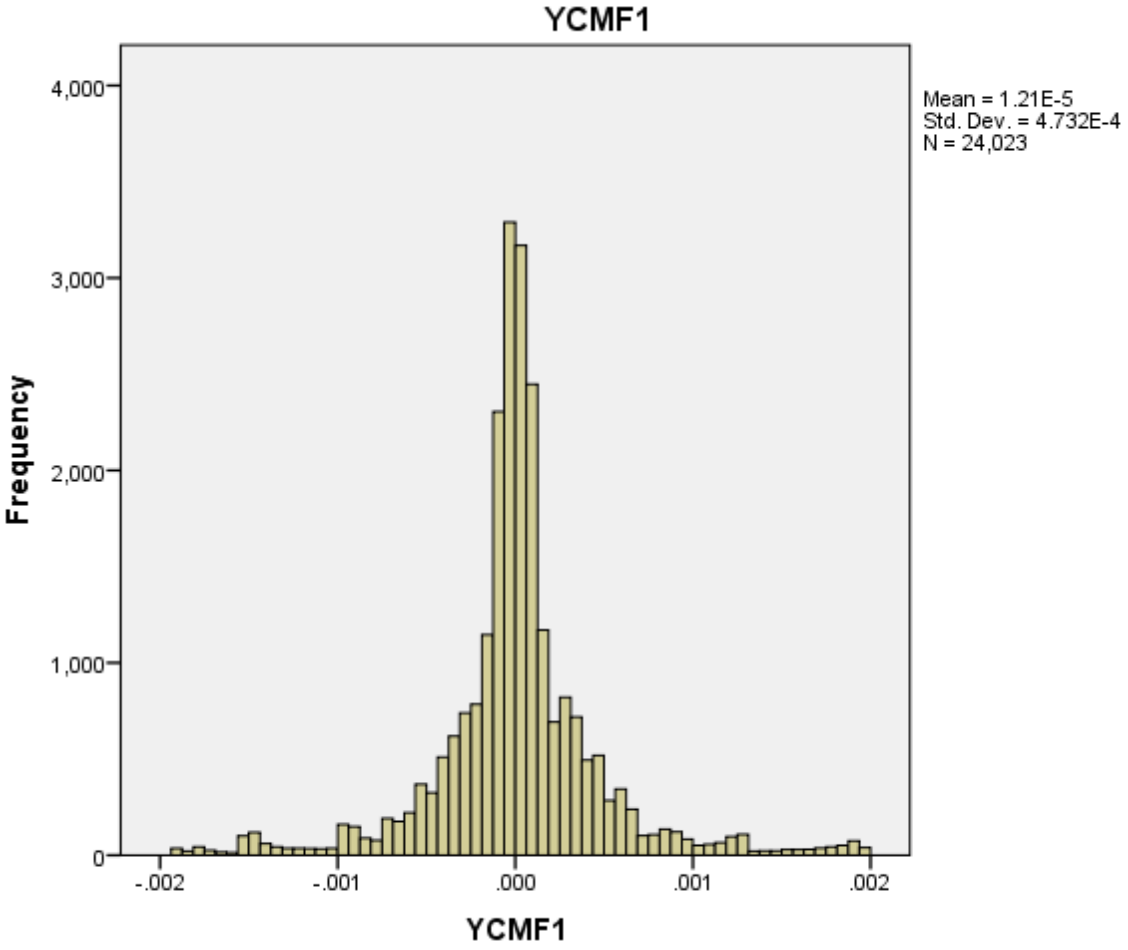

(c) The frequency of CMF1 in the Y direction in Combinedsery1.

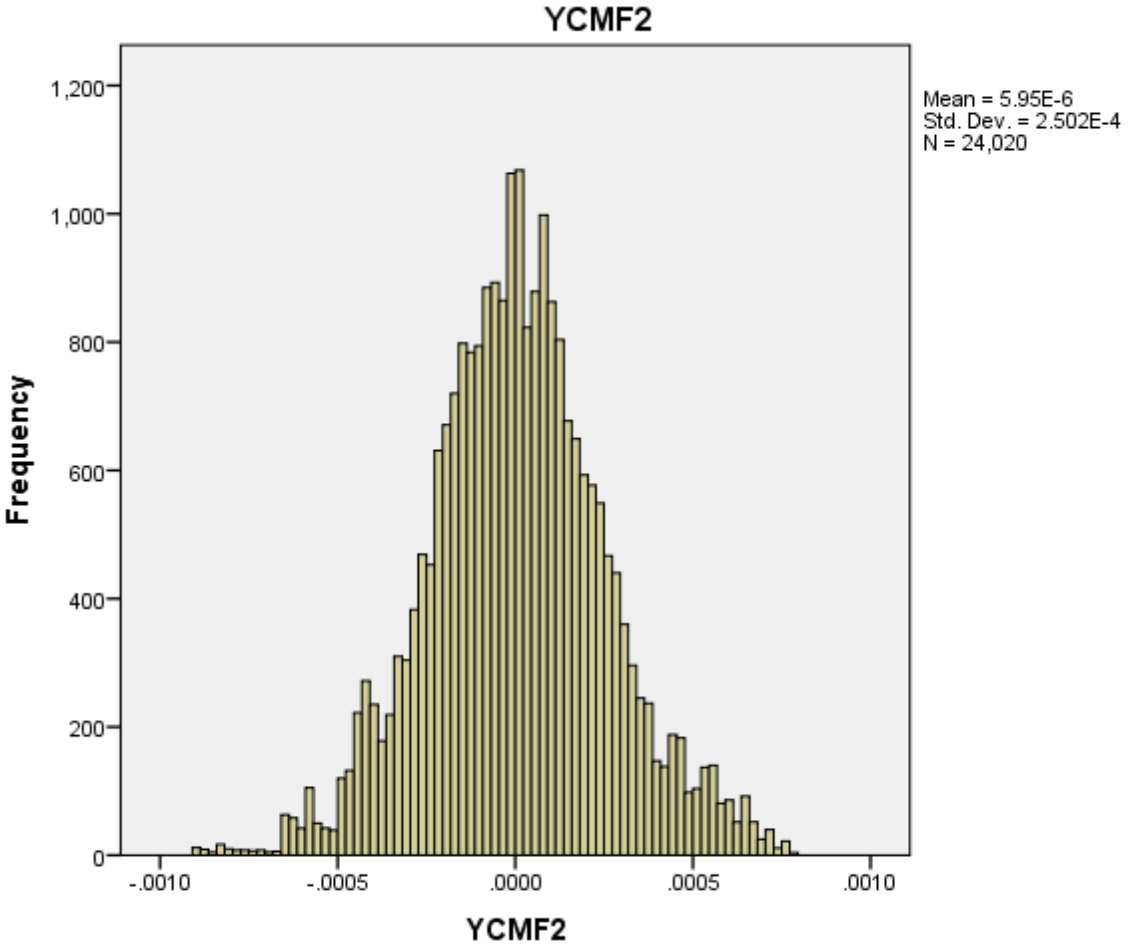

(d) The frequency of CMF2 in the Y direction in Combinedsery1.

Figure 12. The frequency of CMF1 and CMF2 in X and Y directions in Combinedsery1.

BIOGRAPHY

Mehran Akhavan Salmassi graduated in Civil Engineering. He has been working in various fields of projects for more than twenty years. He received his master's degree in structural engineering and currently he is a Ph.D. candidate in structural engineering. He is interested in research in the field of tall buildings and seismic control of structures.

Ali Kheyroddin graduated in Civil Engineering. He received his master's and Ph.D. degree in structural engineering. He is Professor Civil Engineering Faculty Semnan University & Visiting Professor in the University of Texas at Arlington (UTA), Texas, USA (2015). He is interested in research in the field of Reinforced Concrete Structures, Nonlinear Finite Element Analysis of Reinforced Concrete Structures, Tall Buildings (Analysis and Design), Composite Structures, High Performance Fiber Reinforced Concrete (HPFRC), Rehabilitation and Seismic Retrofitting, Progressive Collapse, Neural Networks.

Ali hemmati graduated in Civil Engineering. He received his master's and Ph.D. degree in structural engineering.He is Assistant Professor of structural engineering in Seismic Geotechnical and High Performance Concrete Research Center, Department of Civil Engineering, Semnan Branch, Islamic Azad university. He is interested in research in the field of RC Structures, Seismic Control.